ABSTRACT

HOLLOW FIBER MEMBRANE-BASED AIR GAP MEMBRANE DISTILLATION

by
Xuan Wang

Membrane Distillation (MD) is a thermally-driven separation process. In this research, desalination of 1% NaCl solution is achieved by one type of MD namely, Air Gap Membrane Distillation (AGMD). The characteristics of AGMD are evaluated by using a hollow-fiber-set-based compact device. Hot brine solution and cold water are passed through two different fiber sets separately: porous hydrophobic polyvinylidene fluoride hollow fibers of the E type (PVDF E) and solid polypropylene (PP) hollow fibers. Vapor from the hot brine crosses the membrane pores of the PVDF fibers and the air gap, and finally condenses over the surface of solid hollow fibers. By connecting two or three AGMD modules differently, six different experimental setups are evaluated. Based on the relationship of brine-in temperature, cold water flow rate, water vapor flux and thermal efficiency, the performances of each condition are investigated and evaluated. Enhanced water vapor productivity and thermal efficiency are achieved in small laboratory devices.

HOLLOW FIBER MEMBRANE-BASED
AIR GAP MEMBRANE DISTILLATION

by
Xuan Wang

A Thesis
Submitted to the Faculty of
New Jersey Institute of Technology
in Partial Fulfillment of the Requirements for the Degree of
Master of Science in Pharmaceutical Engineering

Otto H. York Department of
Chemical, Biological and Pharmaceutical Engineering

May 2013

Blank Page

APPROVAL PAGE

HOLLOW FIBER MEMBRANE-BASED AIR GAP MEMBRANE DISTILLATION

Xuan Wang

Dr. Kamalesh K. Sirkar, Thesis Advisor — Date
Distinguished Professor of Chemical Engineering, NJIT

Dr. Boris Khusid, Committee Member — Date
Professor of Chemical Engineering, NJIT

Dr. Xianqin Wang, Committee Member — Date
Assistant Professor of Chemical Engineering, NJIT

BIOGRAPHICAL SKETCH

Author: Xuan Wang

Degree: Master of Science

Date: May 2013

Undergraduate and Graduate Education:

- Master of Science in Pharmaceutical Engineering,
  New Jersey Institute of Technology, Newark, NJ, 2013

- Bachelor of Science in Pharmaceutical Engineering,
  Wuhan Institute of Technology, Wuhan, P. R. China, 2011

Major: Pharmaceutical Engineering

To my parents, 王华强，王莲莲，
For giving me so much support and love in my life

ACKNOWLEDGMENT

Thanks to New Jersey Institute of Technology, I have had the opportunity to pursue my Master's degree here. I appreciate my thesis advisor Professor Kamalesh K Sirkar very much for his constant support and guidance throughout the whole research, which deepens my understanding and cognition about membrane separation.

I am grateful to the members of committee for participating in my thesis. I would like to thank them for their valuable advice and affirmation of my research and achievement.

I am thankful to the help and encouragement from all the members in our research group: Dhananjay, Dengyue, Gordana, Lin, Tripura, Xingming. They provided me with much help and support to continue my experiment. Special thanks to Dhananjay Singh, he guided me in searching for papers on assembling the experiment setup.

Finally, I would like to express my thanks to my parents and relatives. During these two years, they gave me unlimited support and love, which encourages me to face every difficulty. Without both financial and mental support from my parents, I could not accomplish my Master's degree.

TABLE OF CONTENTS

TABLE OF CONTENTS
(Continued)

LIST OF TABLES

LIST OF FIGURES

LIST OF FIGURES
(Continued)

LIST OF SYMBOLS

J	Mass Flux through Membrane, $kgm^{-2}s^{-1}$
P	Vapor Pressure, Pa
N_v	Water Vapor Flux, kg/m^2h
N_p	Number of Porous Hollow Fiber
D_i	Inside Diameter, m
L_p	Length of Porous Hollow Fiber, m
$\dot{H}_c$	Rate of Heat Transfer, cal/h
$\dot{H}_{cd}$	Rate of Heat Removal, cal/h
$\dot{H}_b$	Rate of Heat Loss, cal/h
η	Thermal Efficiency
T_{ci}	Coolant-in Temperature, ºC
T_{co}	Coolant-out Temperature, ºC
T_{ref}	Reference Temperature, ºC
T_{cd}	Condensate Temperature, ºC
T_{bi}	Brine-in Temperature, ºC
T_{bo}	Brine-out Temperature, ºC
$\dot{m}_c$	Coolant Mass Flow Rate, kg/h
$\dot{m}_{cd}$	Condensate Mass Flow Rate, kg/h
$\dot{m}_b$	Hot Brine Mass Flow Rate, kg/h
C_{ci}	Specific Heat of Coolant-in, cal/kgºC

LIST OF SYMBOLS
(Continued)

C_{co}	Specific Heat of Coolant-out, cal/kgºC
T_1	Condensate Temperature from First Module, ºC
T_2	Condensate Temperature from Second Module, ºC
T_3	Condensate Temperature from Third Module, ºC

SUBSCRIPTS

f	Feed
p	Permeate
v	Vapor
m	Membrane

CHAPTER 1

INTRODUCTION

1.1 Membrane Distillation

Membrane Distillation (MD) is a thermally-driven separation process [1]. The temperature difference across porous hydrophobic membrane produces a driving force, the vapor pressure difference. It makes only vapor molecules transfer through the membrane. This separation technology is being widely investigated for potential use in desalination, wastewater treatment and food industry.

1.1.1 Driving Force and Vapor-Liquid Equilibrium

Based on the research of Schofield et al. [2] on factors affecting flux in membrane distillation, different temperatures between the feed and the permeate side leads to different vapor pressures on different sides of the membrane, which becomes a driving force (Figure 1.1). For the simplest expression, the mass flux has a linear relationship with the vapor pressure difference and can be expressed by following equation:

$$J = C(P_f - P_p) \tag{1.1}$$

Here C is a constant somewhat dependent on temperature and pressure; P_f is the vapor pressure at the surface of feed solution; P_p is the vapor pressure at the surface of permeate side.

Lawson and Lloyd suggested two vapor-liquid equilibrium assumptions when modeling the MD process [3]. The first assumption is to ignore kinetic effects at the

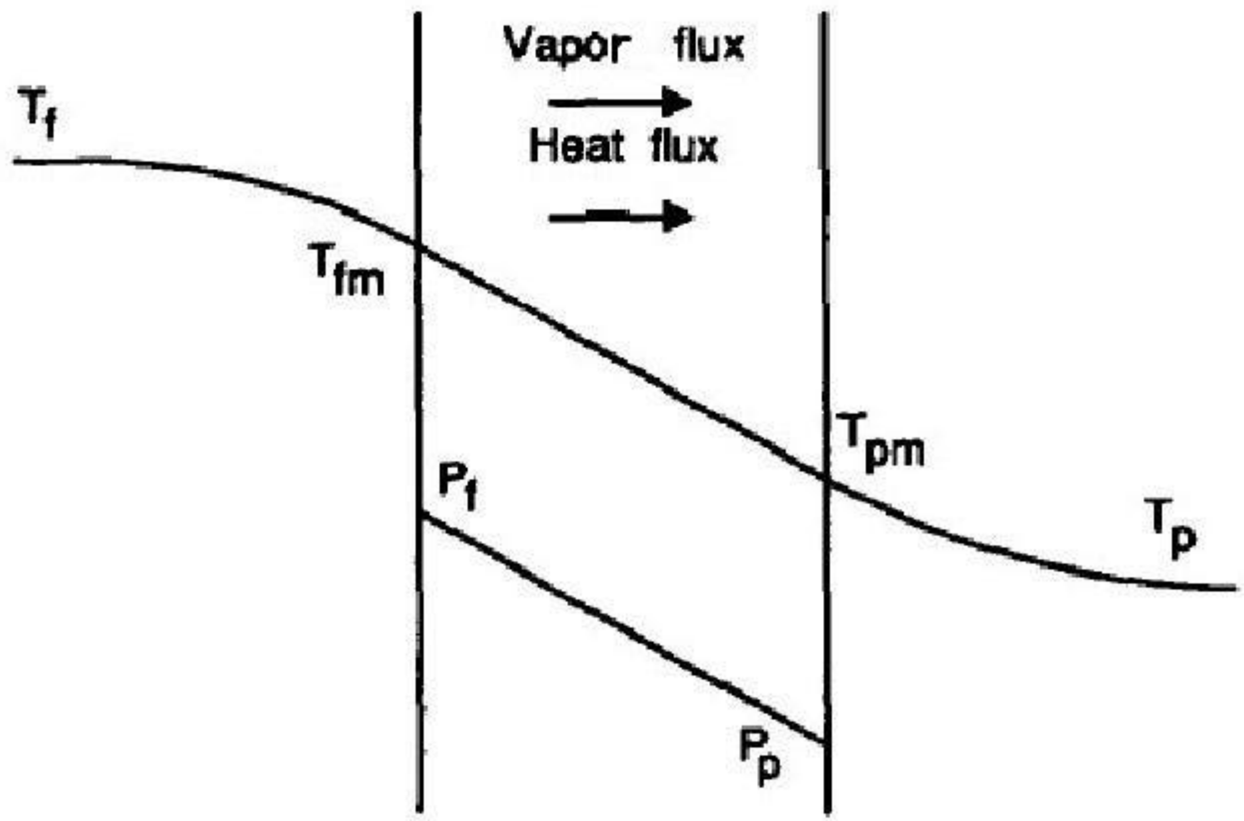

Figure1.1 Temperature profile in membrane distillation [2].

vapor-liquid interface, which means the vapor and liquid are almost in the equilibrium state at the membrane surface as well as the temperature and the pressure. The second one is to ignore the effect of the curvature of the vapor-liquid surface on equilibrium.

1.1.2 Benefits and Drawbacks

MD has many advantages compared with other separation technologies. Firstly, lower external energy and requirement of expenditure of capital and land are important benefits. Secondly, the heat lost from the equipment surfaces to the environment is reduced. That is because the reduced equipment surface area leads to decreased thermal losses in MD. Thirdly, MD is a safer and more efficient separation technology due to the lower operating pressures. It could reject almost 100% solute, like ions, macromolecules, colloids, cells and other non-volatile constituents [3]. MD is a physical separation process, not a chemical one, which makes MD more attractive in industrial applications.

However, MD has some drawbacks. Compared to other separation process, the permeate flux in MD is very low. The heat lost by conduction across the membrane is also a problem.

1.2 Traditional Membrane Modules

Alkhudhiri et al. described traditional membrane modules: these include flat sheet module, tubular module, hollow fiber module, and spiral wound module [1].

- Because flat sheet membranes (Figure 1.2) are easy to remove from membrane modules for cleaning, examination, and replacement, they could be used in characterizing different types of MD membranes. They are popular for laboratory studies.

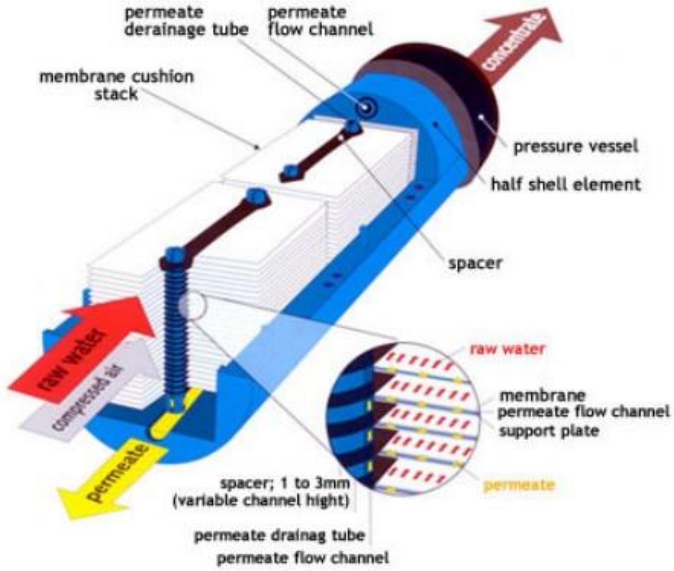

Figure 1.2 The schematic of a flat sheet membrane-based module [4].

- For the tubular module (Figure 1.3), membranes are fixed inside the tube so that they are irreplaceable. But due to their higher membrane surface area and lower boundary layer resistances, they are more productive than flat sheet membranes.

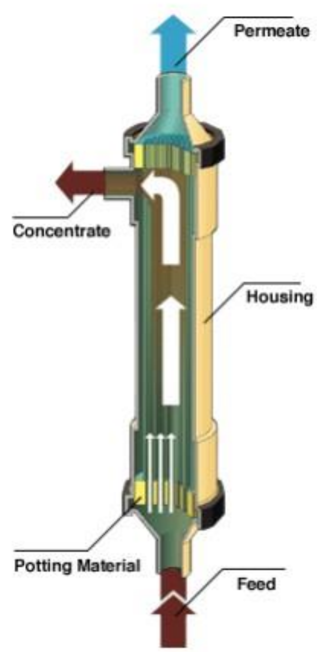

Figure 1.3 The schematic of a tubular module [4].

- For hollow fiber module (Figure 1.4), thousands of hollow fibers are bundled inside a shell tube. The feed solution flows through inside of hollow fibers. Vapor evaporates through the membrane and condenses outside the hollow fibers. Or feed solution flows through the outside of the hollow fibers. Then the condensate is collected from inside of the hollow fibers.

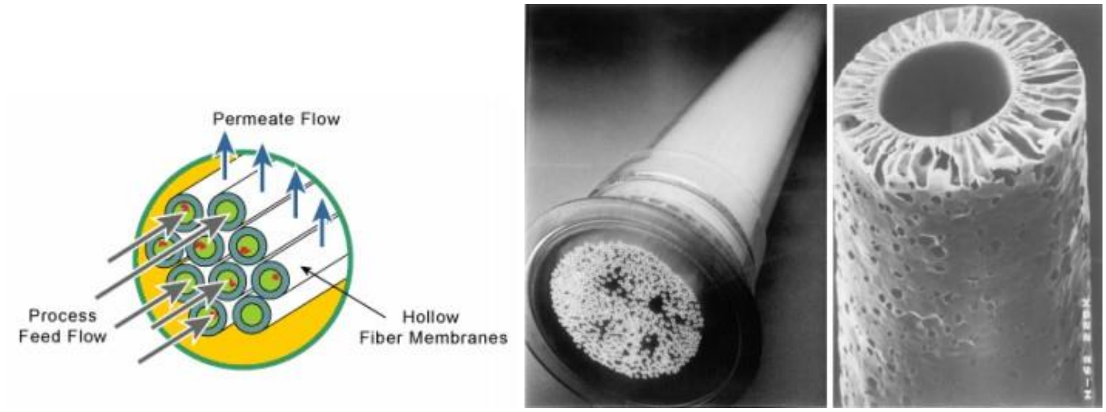

Figure 1.4 The schematic of a hollow fiber module [4].

- In spiral wound module (Figure 1.5), flat sheet membrane and spacers are enveloped and rolled around a perforated central collection tube. Feed solution goes across the membrane surface axially, while permeate solution flows into the center. Finally condensation collects from the central tube [4].

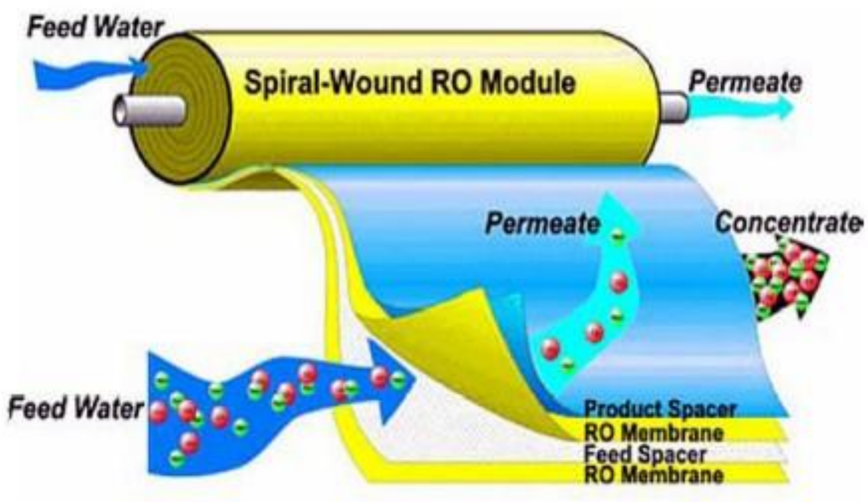

Figure 1.5 The schematic of a spiral wound module [4].

1.3 Four Types of Membrane Distillation

In MD process, one side of the membrane contacts the hot feed solution. The microporous hydrophobic membrane prevents the liquid phase from passing through, which forms a vapor-liquid interface at the surface of the membrane. Volatile compounds evaporate from the feed side. They go through the pore entrance, and finally are condensed on the other side of the membrane [3]. Figure 1.6 illustrates four types of MD configurations based on the different arrangements on the other side of the membrane. They include Direct Contact Membrane Distillation (DCMD), Air Gap Membrane Distillation (AGMD), Sweep Gas Membrane Distillation (SGMD) and Vacuum Membrane Distillation (VMD).

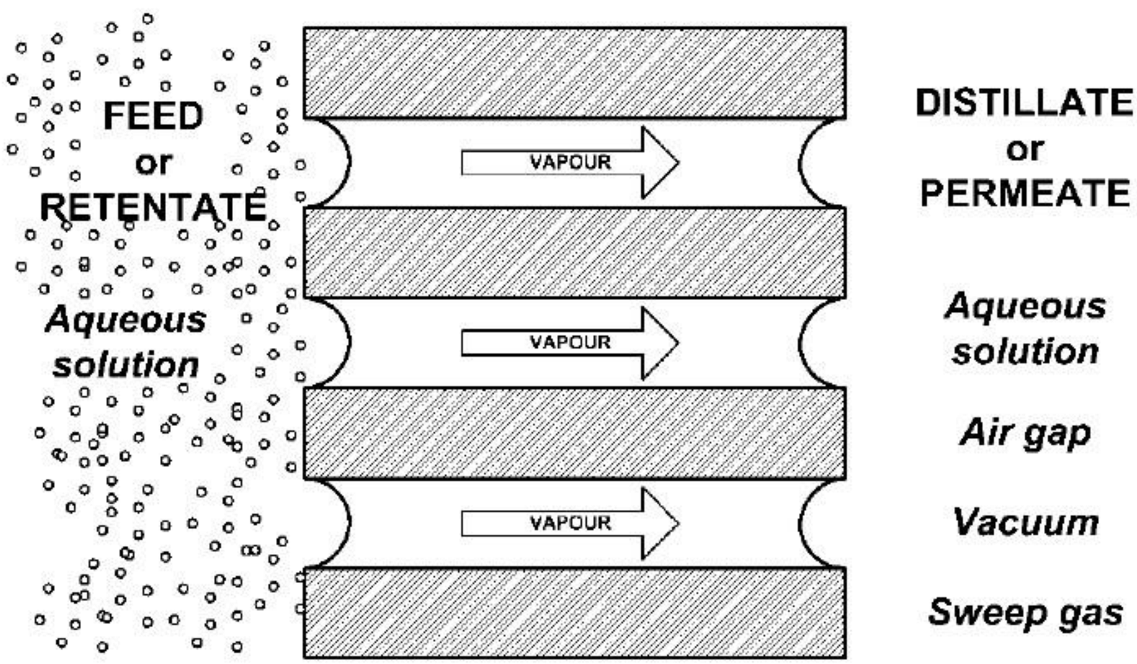

Figure 1.6 A general scheme of the MD process [5].

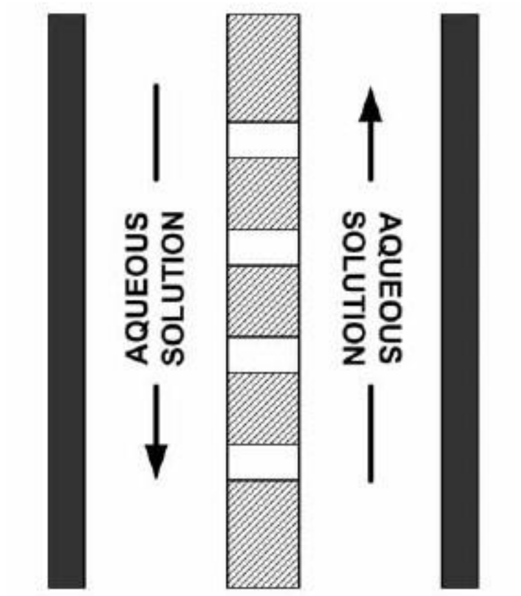

(a) Direct Contact Membrane Distillation.

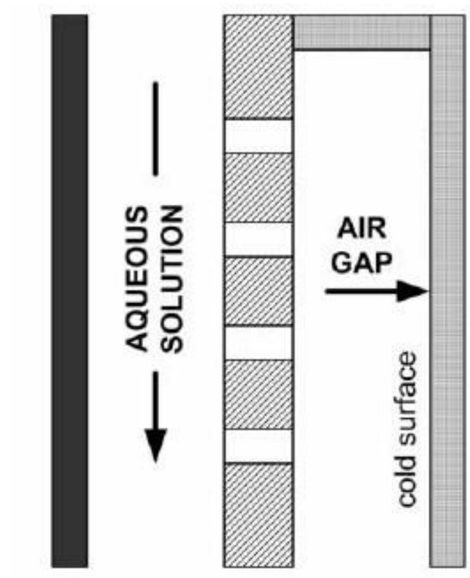

(b) Air Gap Membrane Distillation.

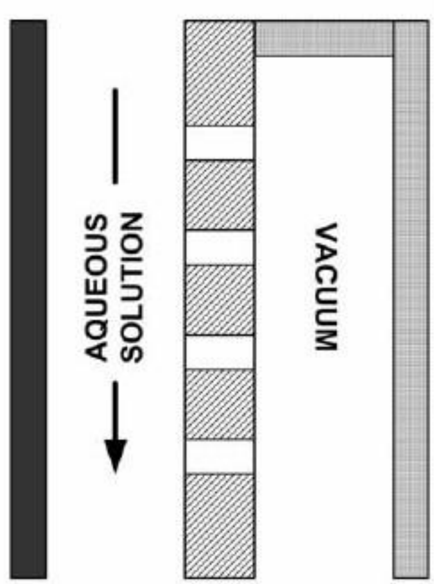

(c) Vacuum Membrane Distillation.

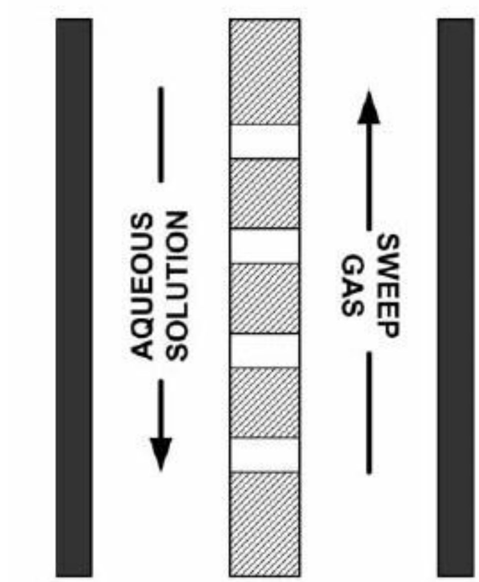

(d) Sweep Gas Membrane Distillation.

Figure 1.7 Configuration of four types of membrane distillation [5]. (a) Direct Contact Membrane Distillation. (b) Air Gap Membrane Distillation. (c) Vacuum Membrane Distillation. (d) Sweep Gas Membrane Distillation.

1.3.1 Direct Contact Membrane Distillation (DCMD)

Figure 1.7 (a) shows the configuration of DCMD. Hot solution and cold solution contact the two sides of the membrane directly. Temperature difference between these two solutions produces vapor pressure difference across the membrane, which makes water evaporate from hot solution and water vapor condenses on the cold solution surface. The feed cannot penetrate the membrane because of the hydrophobic characteristics of membrane.

One of the problems for DCMD is low efficiency during the heat transfer. Large portion of the heat is lost by conduction between the feed solution and the distillate water. In order to solve this problem, placing an air gap between the permeate side and the condensing surface could increase the conductive heat transfer resistance. DCMD can be used in many fields, such as desalination, concentration of aqueous solutions. It can operate under high temperature.

For DCMD, there are many investigations. Findley [6] and Gore [7] have investigated about the need to reduce temperature polarization on the hot brine side. Most studies stated that hydrophobic membranes of polypropylene, polytetrafluroethylene, and polyvinylidene fluoride were used in the DCMD experiment and their characteristics were investigated. Li and Sirkar [8] described that the cross-flow had higher permeate flux than the parallel-flow module in DCMD. Liming Song et al. [9] illustrated a module using the mass transfer coefficient k_m as an adjustable parameter in order to predict the drop of brine temperature, the increase of distillate temperature and water vapor flux. They succeeded to develop a mathematical model to describe and evaluate the performance of the pilot plant with various cross-flow modules.

1.3.2 Air Gap Membrane Distillation (AGMD)

Figure 1.7 (b) shows the configuration of AGMD. Instead of a cold solution, the hot solution and air contact different sides of the membrane directly. There is an air gap between the permeate side of the membrane and the condensing surface. The vapor evaporated crosses the membrane and the air gap, and finally condenses over the cold surface inside the membrane cell.

AGMD does not require a distillate stream. This is a major advantage with respect to DCMD. In this configuration, it also overcomes another DCMD drawback and increases the conductive heat transfer resistance. However, at the same time, this air gap increases the mass transfer resistance and decreases the water vapor flux.

There are many different AGMD module designs. Koschikowski et al. [10] illustrated a spiral-wound module design. For this design, it was composed of three channels, including evaporator channel, distillate channel, and condensate channel. Guijt et al. [11] introduced a design that hot brine passed through the bore of a single porous hollow fiber inside a concentric cylindrical annulus. Outside this, there was a flow of the cold solution. The condensate was obtained from outside the porous hollow fiber. Cheng et al. [12] designed two finned tubular membrane modules. One was the small module having a thin air gap in the grooves of a nonporous finned copper tube. Cold water went through the hollow copper tube. On the outside of the copper tube, a porous PTFE membrane was wrapped around for permeation. The module was made up 10 finned tubes. Singh and Sirkar [13] introduced a two-hollow-fiber-set membrane module. Hot brine solution passed through porous hydrophobic polyvinylidene fluoride hollow fiber set. Cold water entered through the solid polypropylene hollow fiber set. Vapor evaporated from the brine and passed across the membrane and the air gap. Condensation took place on the surface of the solid hollow fibers.

1.3.3 Vacuum Membrane Distillation (VMD)

Figure 1.7 (c) shows the configuration of VMD. Vacuum is created by pump in the permeate membrane side instead of a cold distillate stream in DCMD. Vapor is removed from the membrane module and condensed in a large external condenser. The heat lost by conduction would be negligible in this configuration. However because of the higher pressure difference between the vapor-liquid interface, membrane wetting takes place easily in VMD configuration compared with others. Li et al. [8] stated that high vacuum on the permeate side of membrane in VMD will reduce the conductive heat loss. It means a high water vapor flux can be achieved in VMD. Lawson et al. [3] stated that membrane wetting took place much easily due to higher interface pressure in VMD compared with other MD configuration.

VMD has various applications ranging from environmental waste clean-up to flood processing beside desalination. It includes removal of volatile organic compounds (VOCs) from water, concentration of aqueous solutions and separation of non-volatile components from water. In order to evaluate the effect of membrane compressibility in VMD, and how the performance of the VMD was affected by hollow fiber packing density, module length, feed velocity, vacuum pressure and feed temperature, Lei et al [14], and Curcio and Drioli [5] have carried out many experiments in VMD. The results will serve as a preliminary guide for module design and operational parameter optimization.

1.3.4 Sweep Gas Membrane Distillation (SGMD)

Figure 1.7 (d) shows the configuration of SGMD. Instead of static air in AGMD, inert gas is filled between membrane permeate side and condensate side, and sweeps the vapor to the outside of the membrane cell. Vapor is condensed over the condenser surface of an external condenser.

Flowing inert air will remove volatile compounds from feed solution easily and fast. Similar to AGMD, the air gap reduces the heat loss. But due to flowing inert air, it has high mass transfer resistance. Moreover, large sweep gas is used in removing a small volume of permeate. As a result, permeate process needs a large external condenser, which must do a lot more work.

According to Khayet [15], only 4.5% of the MD papers deal with SGMD. Even though not too many people put many efforts into SGMD, the application of SGMD should not be ignored. He applied it successfully for desalination of aqueous solutions and achieved 100% salt rejection. Boi et al. [16] removed of organics (ethanol, acetone) from waste water successfully by using SGMD.

1.4 Objective

The objective of this work was to explore AGMD process for desalination. A two-set-hollow-fiber-based AGMD module was fabricated for experiment. The first set of hollow fibers has solid wall. The solid hollow fibers of polypropylene (PP) were first used by Zarkadas and Sirkar [17]. The second hollow fiber set consists of porous hydrophobic polyvinylidene fluoride hollow fibers of the E type (PVDF E) [13]. Scanning electron microscope (SEM) micrographs of PVDF E are shown in Figures 1.8, 1.9, and 1.10.

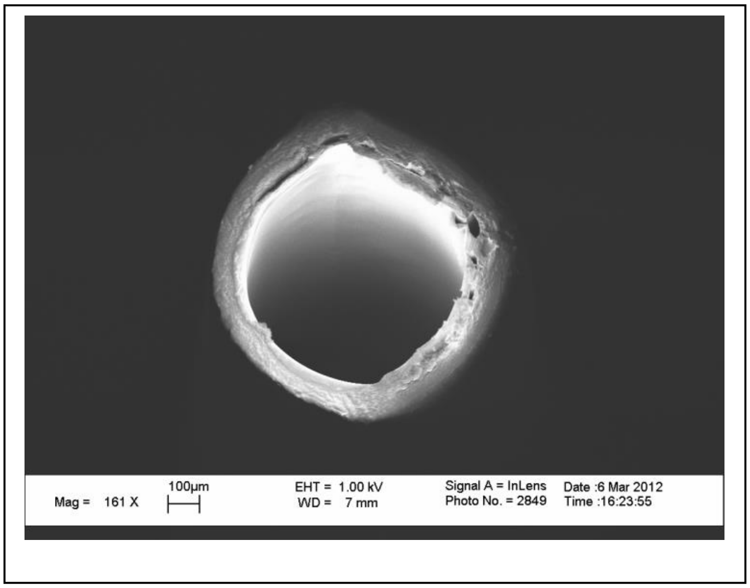

(a)

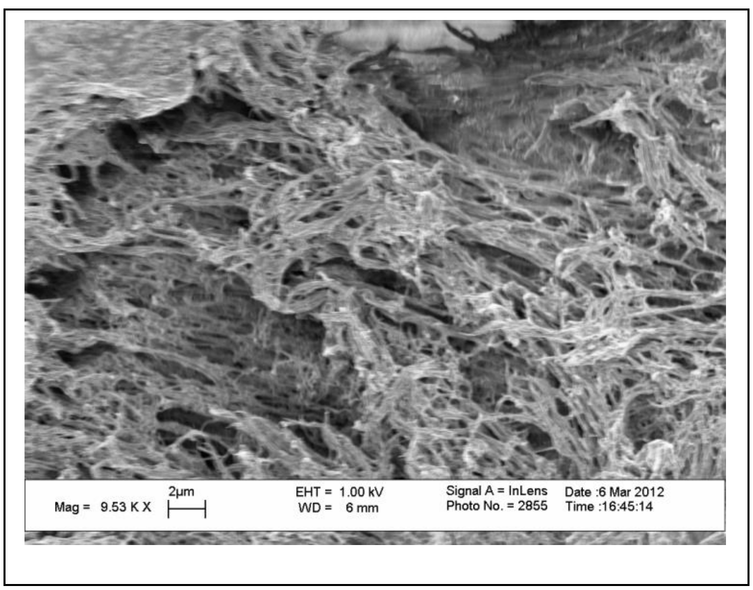

(b)

Figure 1.8 SEM micrographs showing (a) the cross section of PVDF E and (b) structure of wall at 9.5 KX [18].

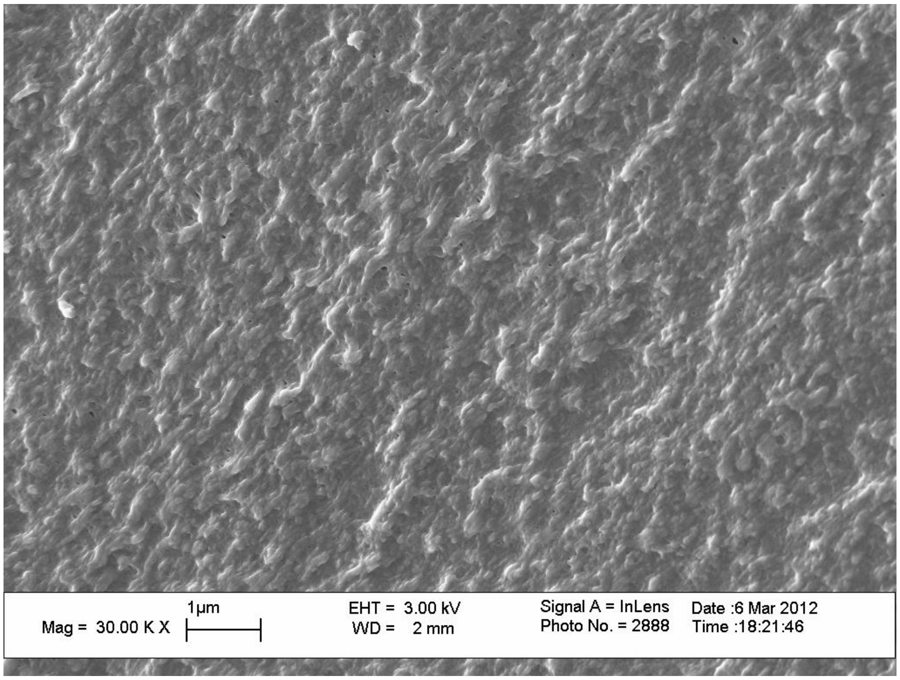

(a)

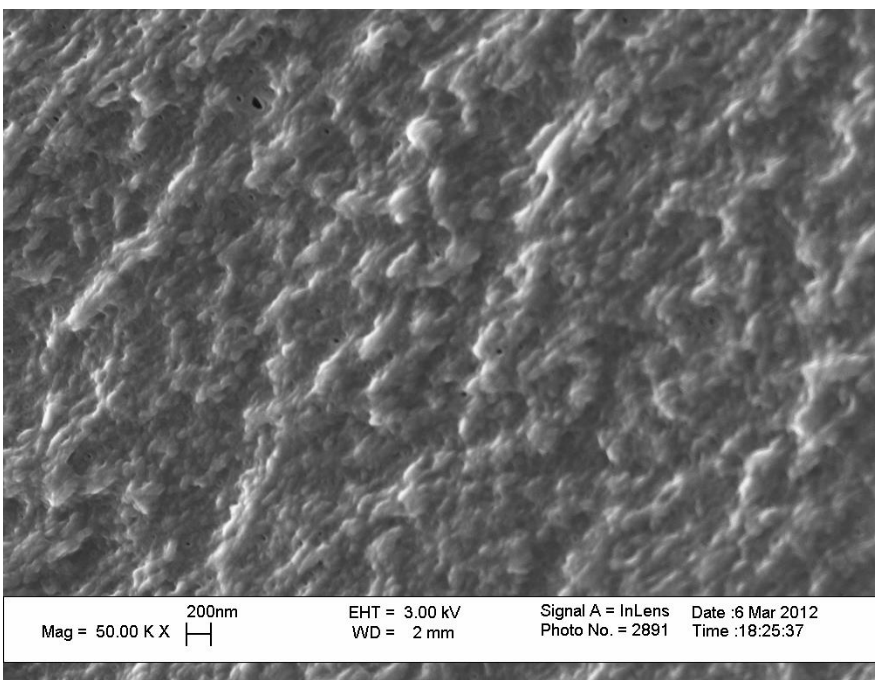

(b)

Figure 1.9 SEM micrographs showing (a) the inner surface of PVDF E at 30.0 KX and (b) the inner surface of PVDF E at 50.0 KX [18].

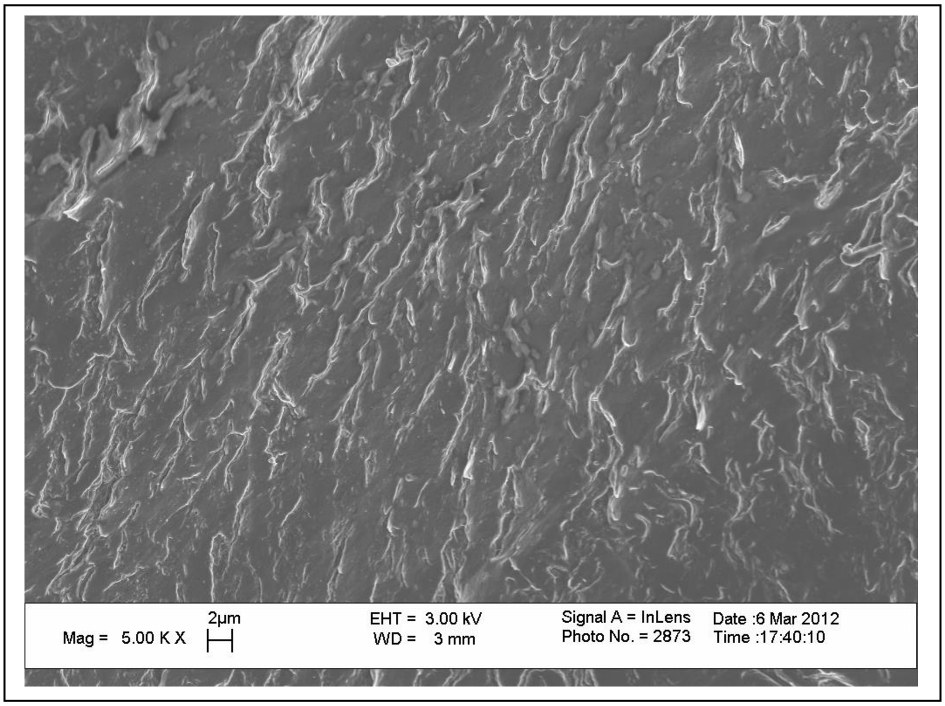

(a)

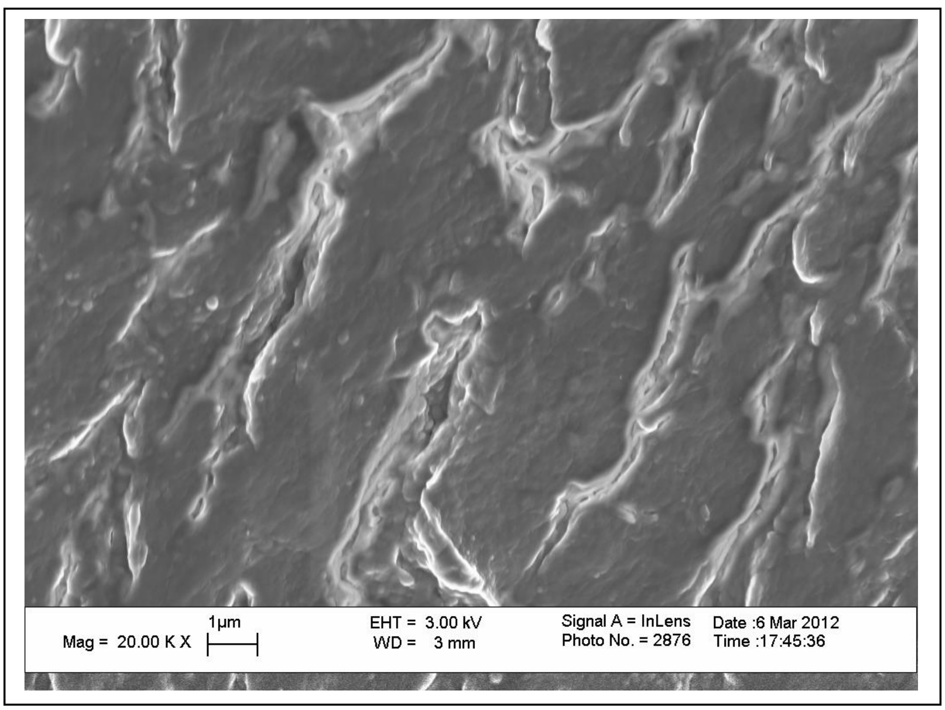

(b)

Figure 1.10 SEM micrographs showing (a) the outer surface of PVDF hollow fiber E at 5.0 KX and (b) the outer surface of PVDF hollow fiber E at 20.0 KX [18].

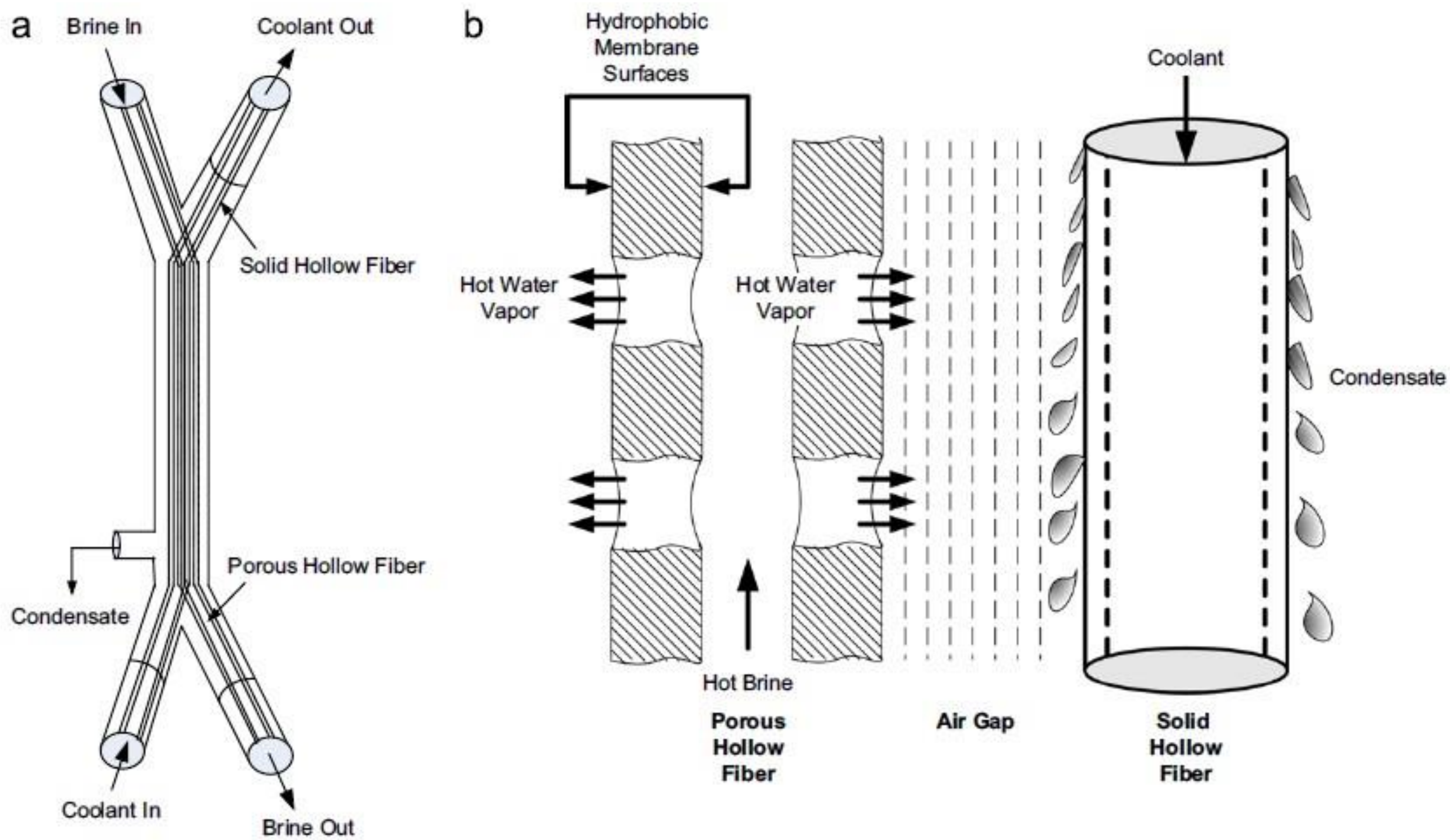

Figure1.11 Schematic of (a) air gap membrane module and (b) air gap membrane process [13].

SEM was used to get images of the topography and structure of PVDF E membrane by scanning it with a focused beam of electrons. These two types of hollow fibers were put into a FEP (Fluorinated Ethylene Propylene) polymer tube. The schematic of an AGMD module is shown in Figure 1.11 (a). The cooling liquid passes through solid hollow fibers, while the hot brine flows through the porous hollow fiber. On the outside of the solid hollow fiber set, water vapor condensation takes place and collects in the bottom of the tube. The whole evaporation process is illustrated in Figure. 1.11 (b).

Generally DCMD processes have higher water vapor flux than AGMD processes. However DCMD process needs a distillate. In this thesis AGMD was used to generate distillate to be used in a two-hollow-fiber-set module with a configuration of DCMD and AGMD. The behavior of the overall configuration of AGMD-DCMD was studied.

CHAPTER 2

MATERIALS AND METHODS

2.1 Experimental Setup

The schematic of the experimental setup is shown in Figure 2.1. 1% NaCl solution was heated in the brine tank. The hot brine was passed through the prefilter to remove trace impurities. Then it was passed through porous hollow fibers. On the cold water side, deionized water was pumped into the bore of the solid hollow fibers in a countercurrent direction. The membrane modules were fastened vertically by iron stands with the hot brine and the cooling water entering at different ends. The distillate water was condensed on the outer surface of the solid hollow fiber and collected from the bottom of the module. The inlet flow rate of the hot brine was maintained at 76 ml/min or 53 ml/min. The inlet flow rate of cooling water was changed from 5 ml/min to 50 ml/min. The temperatures of brine stream, cold stream, and the condensed stream were measured by thermocouples and monitored by thermometer. The conductance of the condensate was monitored by a conductivity meter. The actual experimental setup is shown in Figure 2.2.

2.2 Materials and Chemicals

2.2.1 Membranes

The properties of porous and solid hollow fibers in the AGMD membrane modules are listed in Table 2.1. PVDF E porous hollow fibers were obtained from Arkema Inc., King of Prussia, PA. PP solid hollow fibers were purchased from Celgard, Chrlotte, NC.

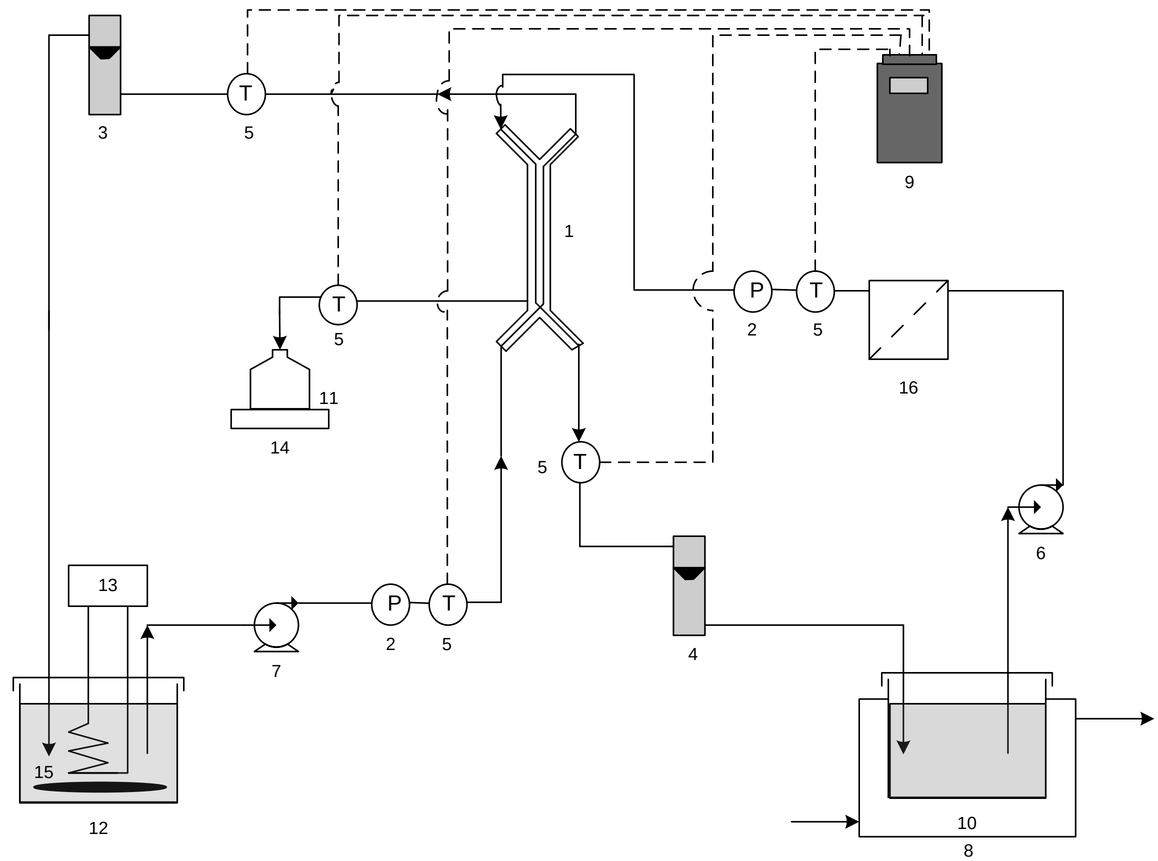

Figure 2.1 Experimental setup for hollow fiber membrane-based AGMD system. 1. Membrane module; 2. Pressure indicator; 3. Coolant flowmeter; 4. Brine flowmeter; 5. Thermocouple; 6. Hot brine pump; 7. Coolant pump; 8. Constant temperature bath; 9. Thermometer; 10. Hot brine tank; 11. Condensate reservoir; 12. Magnetic stirrer; 13. Chiller; 14. Weight balance; 15. Coolant tank; 16. Prefilter.

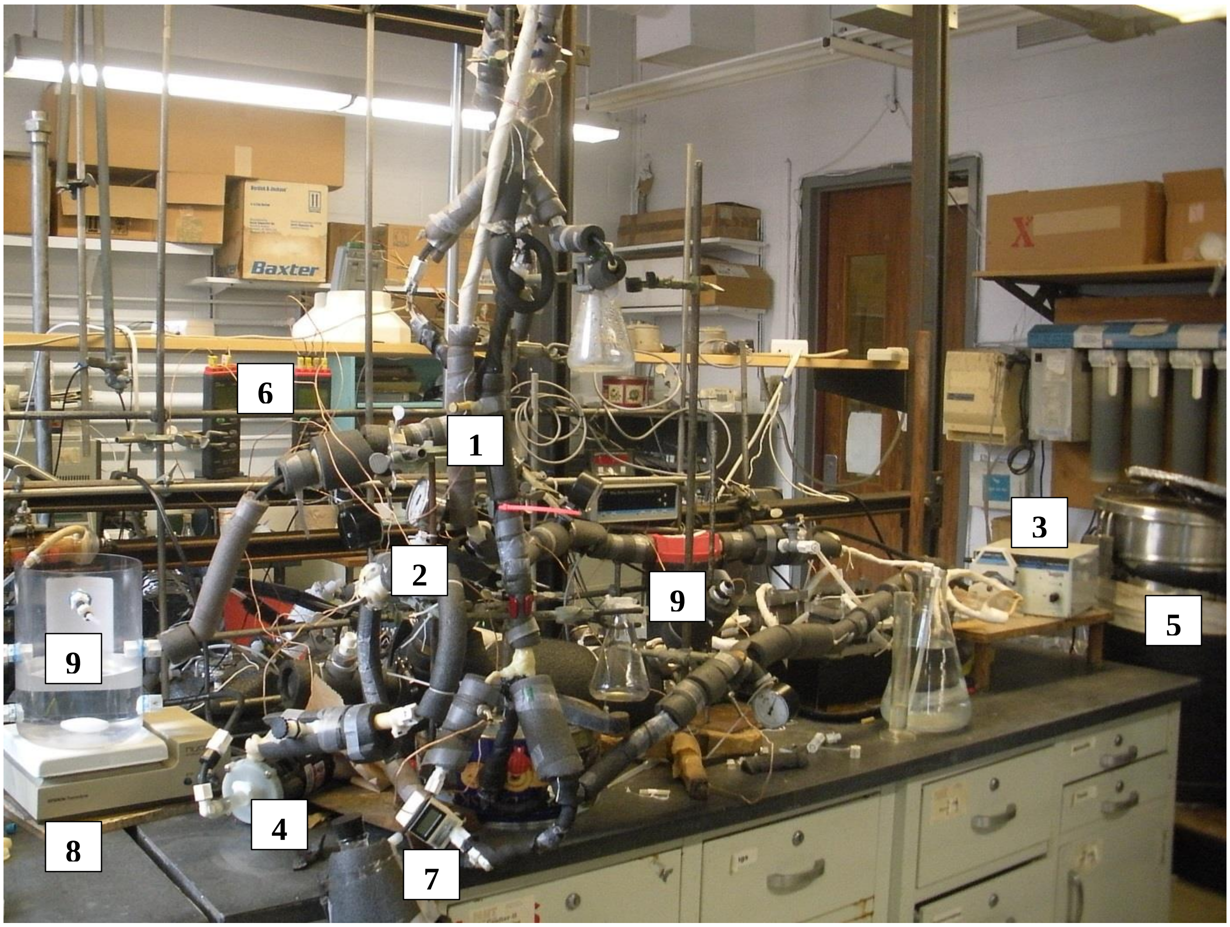

Figure 2.2 The picture of experimental setup for hollow fiber membrane-based AGMD system. 1. Membrane module; 2. Thermocouple; 3. Hot brine pump; 4. Coolant pump; 5. Feed tank; 6. Thermometer; 7. Condensate reservoir; 8. Magnetic stirrer; 9. Coolant tank; 10. Prefilter.

Table 2.1 Characteristics of Solid and Porous Hollow Fiber Membranes

Membrane	Outside diameter of hollow fiber (μm)	Inside diameter of hollow fiber (μm)	Wall thickness (μm)	Pore size (μm)	Porosity
PVDF E	925	691	117	0.2	0.54
PP	575	420	-	-	-

Table 2.2 Details of Three AGMD Modules

Membrane	No. of porous hollow fibers	No. of solid hollow fibers	Length (cm)	Inside diameter of porous hollow fiber (μm)	Inside surface area of porous hollow fibers (cm^2)	Outside surface area of porous hollow fibers (cm^2)
Module #1	7	24	36.8	691	55.89	74.82
Module #2	7	35	15.5	691	23.54	31.51
Module #3	7	24	40	691	60.75	81.33

2.2.2 Chemicals

- NaCl (SIGMA-ALDRICH Co., St. Louis, MO)
- Deionized water
- Activator D (Armstrong epoxy adhesives. Resin Technology Group, Easton, MA)
- C – 4 resin (Armstrong epoxy adhesives. Resin Technology Group, Easton, MA)
- Loctite M-21HP Hysol Medical device epoxy adhesive.

2.2.3 Instruments

- Heater (George Ulanet Company, Newark, NJ)
- Diqi-Sense Temperature Controller (Eutech Instruments Pte Ltd., Singapore)
- Prefilter
- Masterflex Pump Controller module 7518-10 (Cole Parmer Instrument Co.)
- Pump MDX-3 (March MFG. Inc., Glenview, ILL.)
- Conductivity Meter (Model Orion 115+, Thermo, Vernon Hills, IL)
- Thermometer (SPER SCIENTIFIC 800023, 4 Channel Thermometer)
- Nuova II Stirrer Sybron Thermolyne
- CH 3000 Series Chiller, Remcor Liquid Cooling Systems

2.3 Fabrication of Membrane Modules

2.3.1 Preparation of Epoxy Resin

$$\mathrm{C} - 4\ \mathrm{Resin} + \mathrm{Activator\ D}\ \rightarrow \mathrm{Epoxy\ Resin}$$

C − 4 resin and activator D were mixed by mass ratio 4:1. After stirring for several minutes, epoxy resin was mixed completely. It was kept in the fume cupboard for about 5-10 minutes to make it more viscous.

2.3.2 Fabrication of Membrane Module

Table 2.1 lists the characteristics of two hollow fiber membranes and Table 2.2 states the details of three AGMD modules. The pictures of the AGMD modules are shown in Figures 2.3 and 2.4. FEP polymer tube (Cole Parmer, Vernon Hills, IL) having an inside diameter of 1.4 cm was used as the shell of the module. At each end of this shell, two Y-fittings having an inside diameter of 1cm were connected by epoxy resin. The resin was left to cure for at least 24 h. After the shell of module was already prepared, porous hollow fibers and solid hollow fibers were placed inside. Each arm of the Y-fitting was sealed up by plugging with epoxy. On the other hand, the porous PVDF fibers were somewhat larger. Few of these fibers along with a much larger number of solid hollow fibers were used. Module #2 had one shell-side opening. However, modules #1 and #3 had two shell-side openings at two ends of the modules.

Figure 2.3 The picture of AGMD module with one shell-side opening.

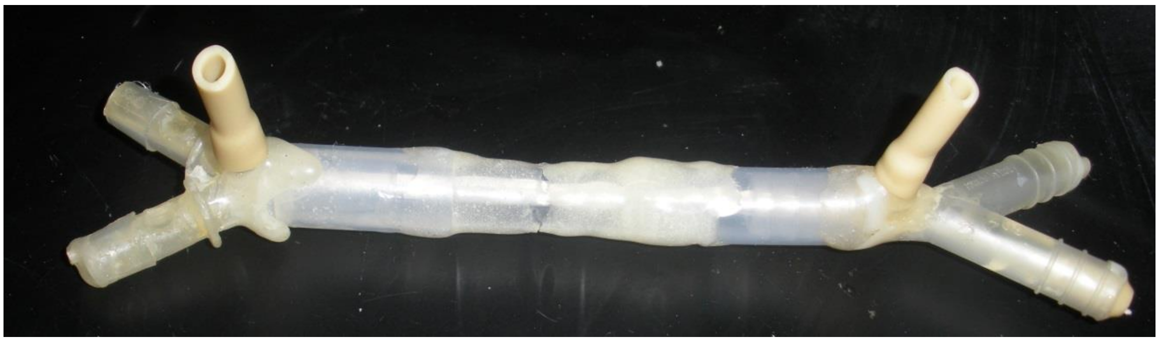

Figure 2.4 The picture of AGMD module with two shell-side openings.

2.4 Calculations

2.4.1 Water Vapor Flux

Water vapor flux was calculated under steady state. The following assumptions were made. The brine flow rate, the cold water flow rate, the brine in temperature, the brine out temperature, the coolant in temperature and coolant out temperature were constants during the experiment. Small fluctuations in these data are ignored. The distillate water collected in the condensate tank over a certain time was used for calculation of water vapor flux (N_v) from following equation:

$$N_v(\mathrm{kg/m^2h}) = \frac{\text{volume of water transferred (L)} \times \text{density of water (kg/L)}}{\text{membrane surface area (m}^2\text{)} \times \text{time(h)}} \qquad (2.1)$$

The surface area of the porous hollow fiber membrane based on inside diameter can be expressed by following relation:

$$\text{Membrane area} = N_p \, \pi \, D_i \, L_p \tag{2.2}$$

Here N_p is the number of porous hollow fibers, D_i is the inside diameter of porous hollow fiber (m), L_p is the length of the porous hollow fiber (m).

2.4.2 Thermal Efficiency

Generally, thermal efficiency is the ratio between the useful output of a system and the input energy. In AGMD, thermal efficiency of the system was calculated under steady state. Thermal efficiency was defined as the sum of the rate of enthalpy transfer to the coolant fluid and the rate of enthalpy exit associated with the condensed liquid divided by the rate of enthalpy loss by brine. In order to get thermal efficiency, each enthalpy equation can be expressed as follows.

The rate of heat transfer to the coolant fluid is:

$$\dot{H}_c = \dot{m}_c \, (C_{co} - T_{ref}) - C_{ci} \, (T_{ci} - T_{ref}) \tag{2.3}$$

Here $\dot{m}_c$ is the cooling water mass flow rate (kg/h), C_{co} is specific heat of coolant-out (cal/kg˚C), C_{ci} is specific heat of coolant-in (cal/kg˚C), T_{co} is coolant-out temperature (˚C), T_{ci} is coolant-in temperatures(˚C), T_{ref} is the reference temperature (˚C) which is assumed to be room temperature (20˚C).

The rate of heat removal associated with the condensed liquid is as follows:

$$\dot{H}_{cd} = \dot{m}_{cd} \, (C_{cd} - T_{cd} \; - C_{ref} \, T_{ref}) \tag{2.4}$$

Here $\dot{m}_{cd}$ is the condensate mass flow rate (kg/h), C_{cd} is specific heat of condensate (cal/kg˚C), C_{ref} is specific heat at reference temperature (cal/kg˚C), T_{cd} is condensate temperature (˚C) and T_{ref} is reference temperature (˚C).

The rate of heat loss from the hot brine solution is expressed as

$$\dot{H}_{b} = \dot{m}_{b} \, (C_{bi} \, (T_{bi} - T_{ref}) - C_{bo} \, (T_{bo} - T_{ref})) \tag{2.5}$$

Here $\dot{m}_{b}$ is the hot brine mass flow rate (kg/h), C_{bi} is the specific heat of brine in (cal/kg˚C), C_{bo} is the specific heat of brine out (cal/kg˚C), T_{bi} is brine in temperature (˚C), T_{bo} is brine out temperature (˚C).

Based on the above equations, the thermal efficiency is calculated by the following:

$$\eta = (\dot{H}_{c} + \dot{H}_{cd}) \, / \, \dot{H}_{b}$$

$$= \frac{\dot{m}_{c} (C_{co} (T_{co} - T_{ref}) - C_{ci} (T_{ci} - T_{ref})) + \dot{m}_{cd} (C_{cd} T_{cd} - C_{ref} T_{ref})}{\dot{m}_{b} (C_{bi} (T_{bi} - T_{ref}) - C_{bo} (T_{bo} - T_{ref}))} \tag{2.6}$$

CHAPTER 3

RESULTS AND DISCUSSION

3.1 Influence of Brine-in Temperature on the Water Vapor Flux

Under different conditions, water vapor flux increases with the rise of brine-in temperature when the temperature was varied from 53.5 ˚C to 80 ˚C.

- **Condition 1.** Evaluate the performance characteristics of only Module #1. From Figure 3.1, hot brine solution goes through the module #1 from the top; cold water enters from the opposite direction.

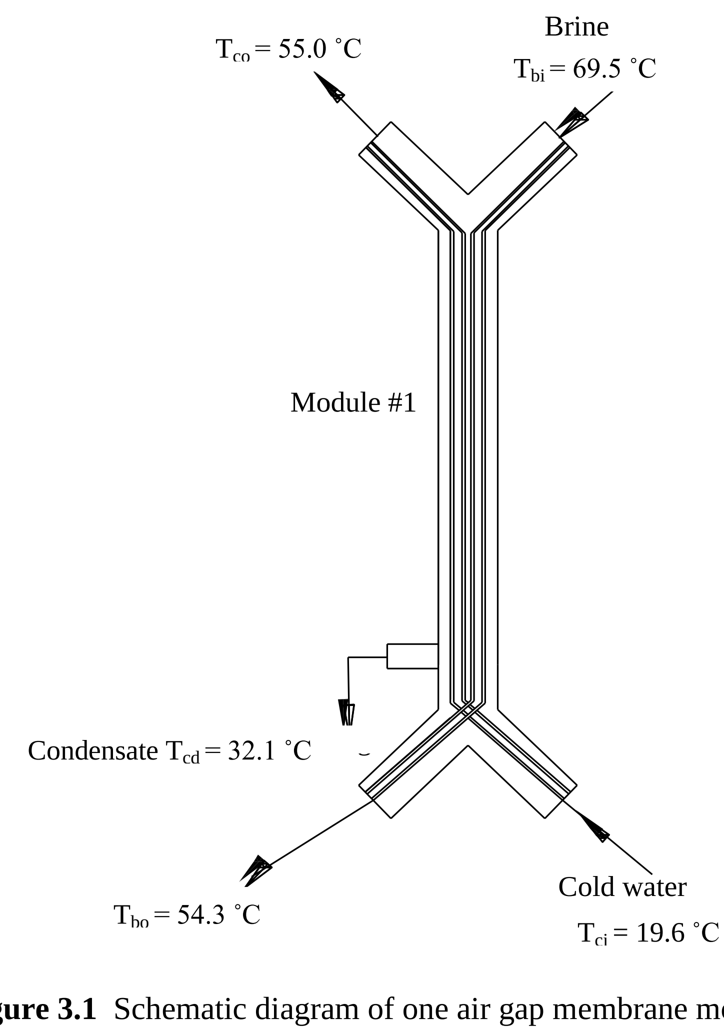

Figure 3.1 Schematic diagram of one air gap membrane module.

- **Condition 2.** Evaluate the performance characteristics of Modules #1 and #2. From Figure. 3.2, the brine solution flows in through the top of module #1 and then enters the module #2 from the bottom. Cold water goes in the opposite direction through the bottom of module #1 in countercurrent flow and then through the top of module #2. Two modules are connected with each other in series.

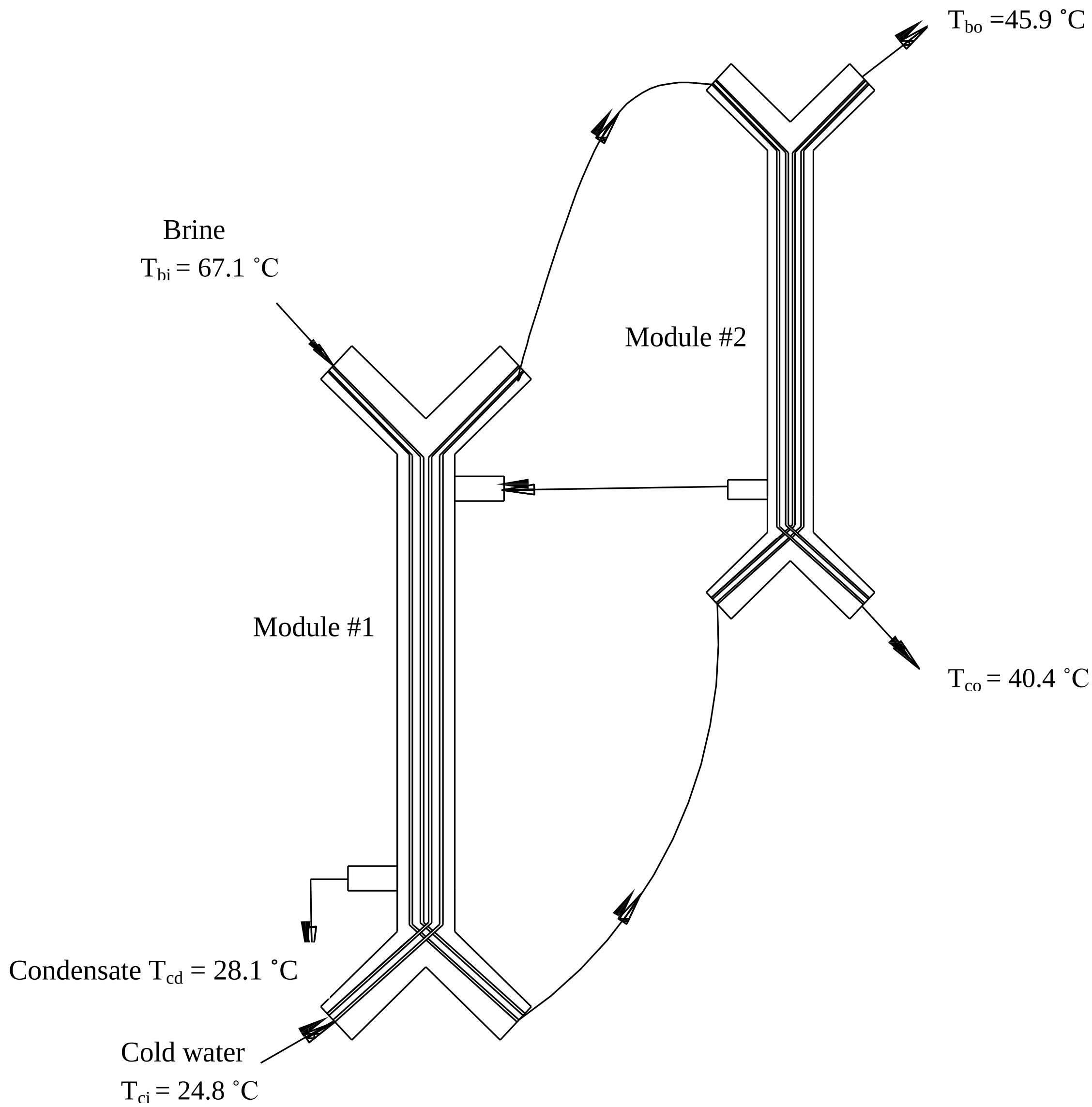

Figure 3.2 Schematic diagram of two air gap membrane modules connected as in Condition 2.

- **Condition 3.** In Figure 3.3, the brine solution flows in through the top of module #1 and then module #2. Cold water goes in the opposite direction through the bottom of module #2 in countercurrent flow and then through module #1. Two modules are connected with each other in series.

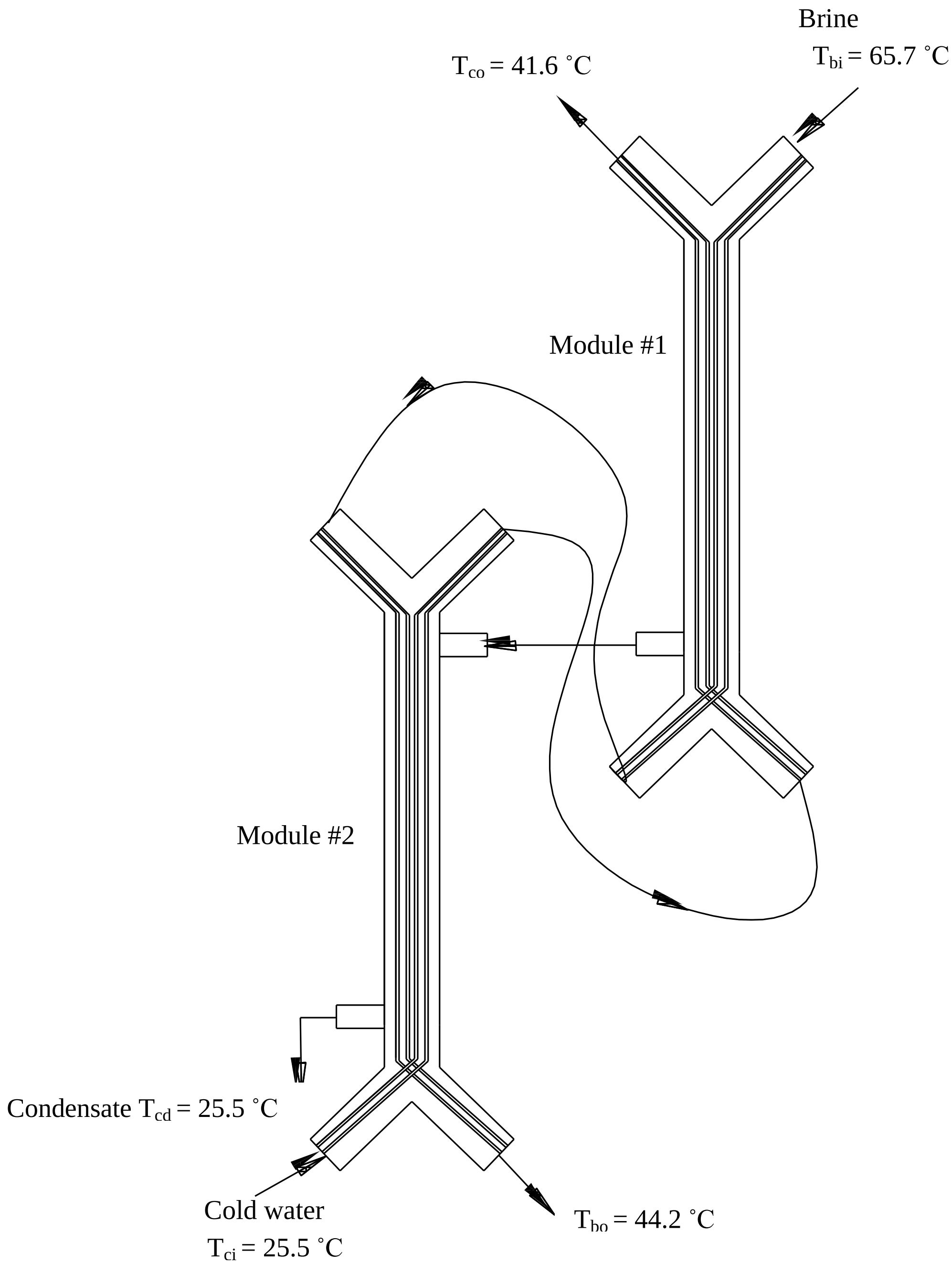

Figure 3.3 Schematic diagram of two air gap membrane modules connected per Condition 3.

- **Condition 4.** In Figure 3.4, the brine solution flows in through the top of module #1 and then enters the module #3 from the bottom. Cold water goes in countercurrent direction from the top of module #3 and through module #1 from the bottom. Two modules are connected with each other in series.

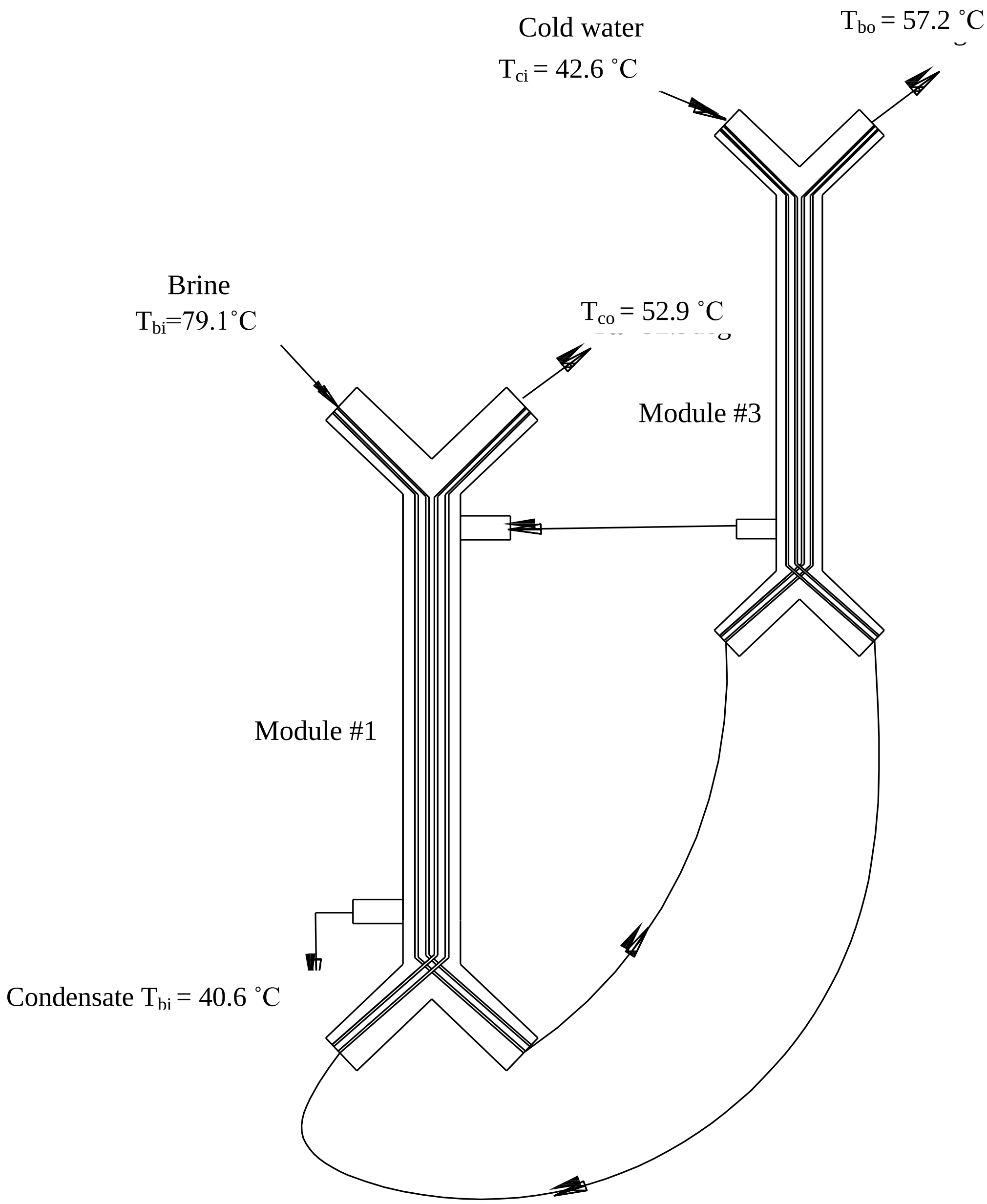

Figure 3.4 Schematic diagram of two air gap membrane modules connected per Condition 4.

- **Condition 5.** In Figure 3.5, the brine solution flows in through the bottom of these three modules. Cold water goes in countercurrent direction from the top. Three modules are connected with one another in series.

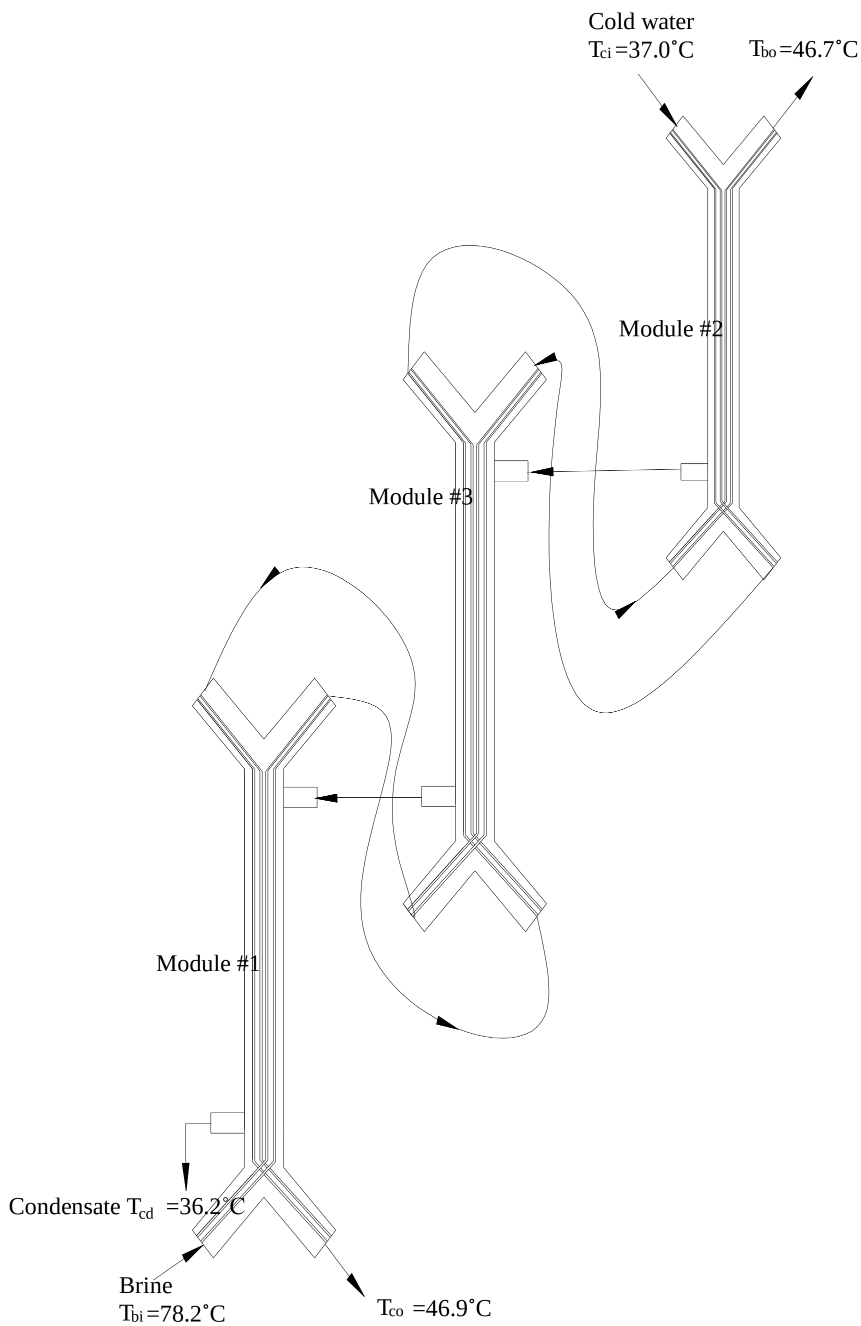

Figure 3.5 Schematic diagram of three air gap membrane modules connected per Condition 5.

- **Condition 6.** In Figure 3.6, the brine solution flows in through the top of these three modules. Cold water goes in the countercurrent direction from the bottom. Three modules are connected with one another in series.

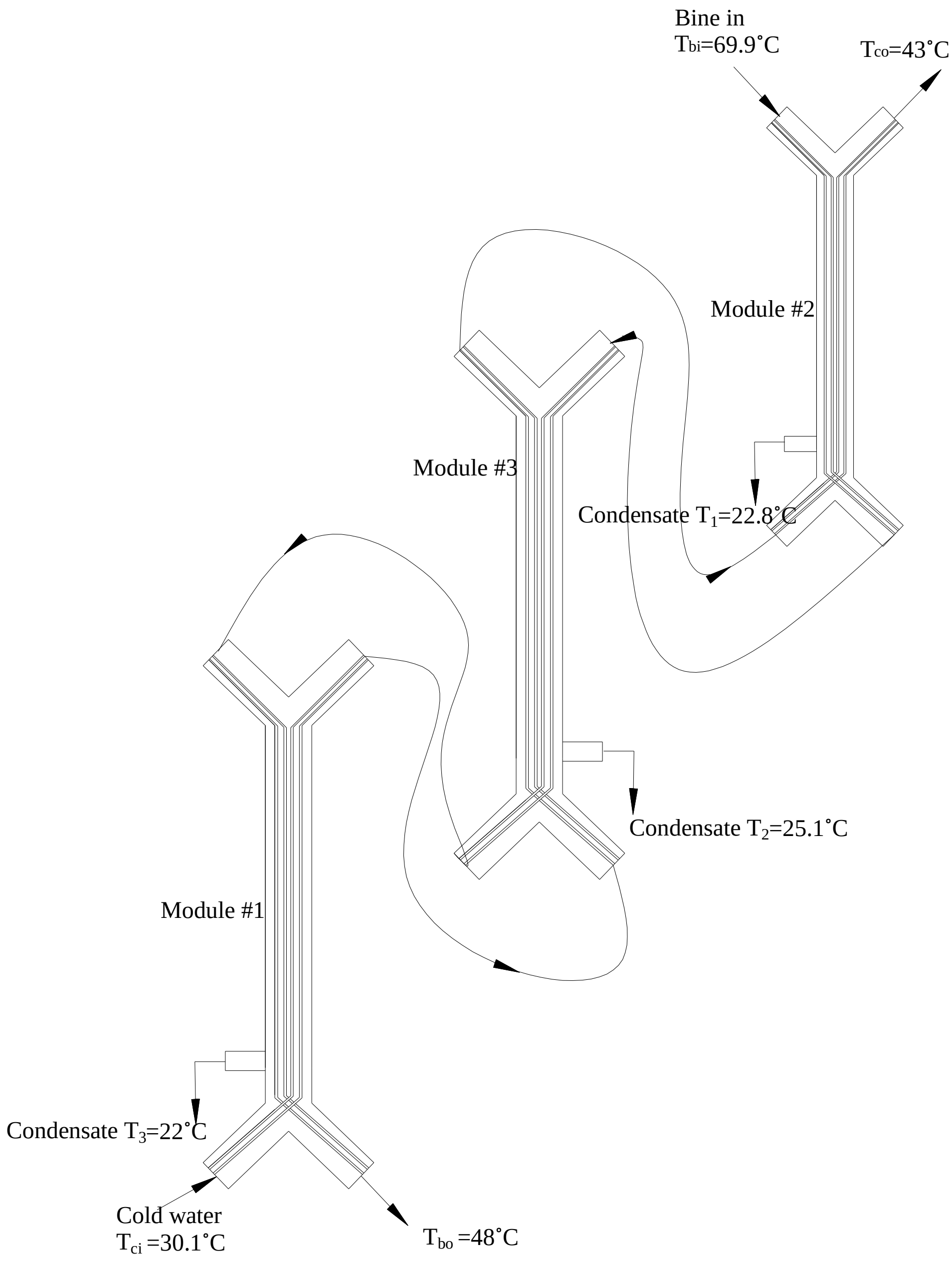

Figure 3.6 Schematic diagram of three air gap membrane modules connected per Condition 6.

3.1.1 Condition 1

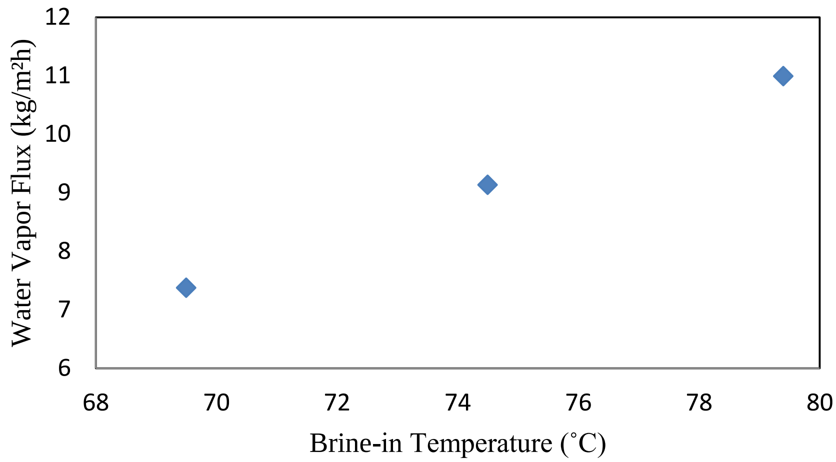

Figure 3.7 In Condition 1, the effect of brine-in temperature on water vapor flux.

For Condition 1, only one module was used for AGMD equipment. Hot brine was passed through the bores of porous hollow fibers at a flow rate of 76 ml/min. Cold water was flowing through the bores of solid hollow fibers at the rate of 50 ml/min. The cold water in temperature was maintained at about 20 ˚C for all AGMD experiments. Water vapor flux increased from 7.37 kg/m^2h to 10.99 kg/m^2h as the temperature of brine was increased from 69.5 ˚C to 79.4 ˚C as shown in Figure 3.7. From Table A.1, the thermal efficiency was around 50% for all the AGMD experiments shown in Condition 1.

3.1.2 Condition 2

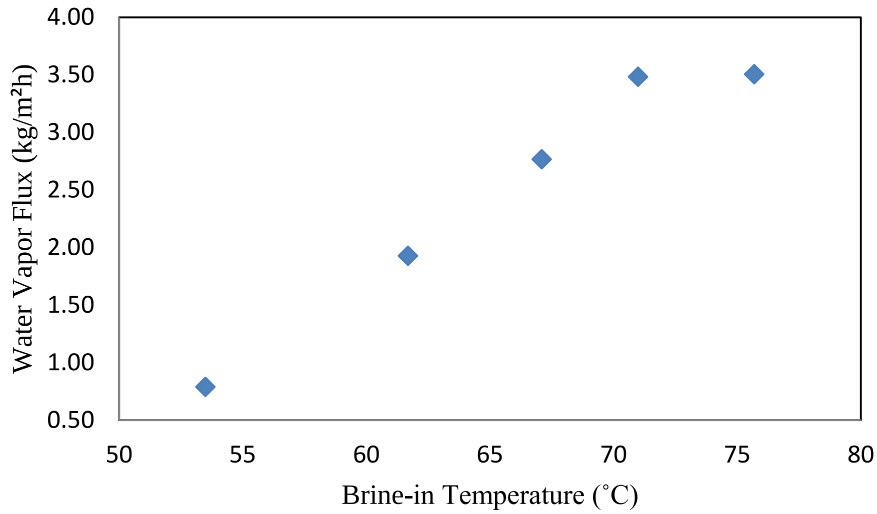

Figure 3.8 In Condition 2, the effect of brine-in temperature on water vapor flux.

For Condition 2, Modules #1 and #2 were used for AGMD and AGMD-DCMD operating configuration seperately. Hot brine was passed through the bores of porous hollow fibers at a flow rate of 76 ml/min. Cold water was flowing through the bores of solid hollow fibers at the rate of 50 ml/min. The cold water temperature was maintained at about 24 ˚C for all AGMD experiments. Water vapor flux increased from 0.79 kg/m^{2}h to 3.50 kg/m^{2}h as temperature of brine was increased from 53.5 ˚C to 75.7 ˚C as shown in Figure 3.8. From Table A.2, the thermal efficiency was around 50% for all the AGMD experiments shown in Condition 2. The highest thermal efficiency was 54% achieved at 75.7 ˚C brine in temperature, which was higher than that for one module in Condition 1.

3.1.3 Condition 3

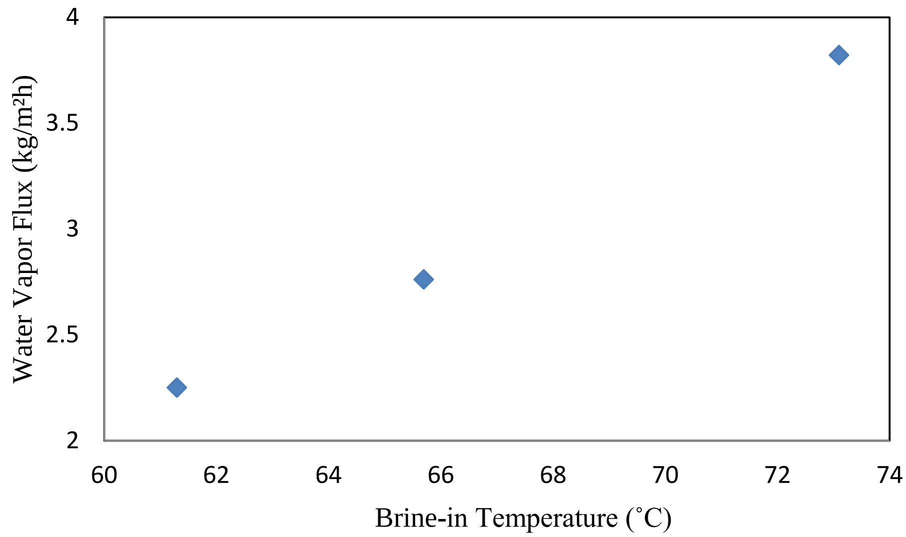

Figure 3.9 In Condition 3, the effect of brine-in temperature on water vapor flux.

For Condition 3, Modules #1 and #2 were used for AGMD and AGMD-DCMD configuration separately but connected to each other differently. Hot brine was passed through the bores of porous hollow fibers at the flow rate of 76 ml/min. Cold water was flowing through the bores of solid hollow fibers at the rate of 50 ml/min. Cold water temperature was maintained at about 25 ˚C for all AGMD experiments. Water vapor flux increased from 2.17 kg/m^{2}h to 3.82 kg/m^{2}h as the temperature of brine increased from 61.3 ˚C to 73.1 ˚C as shown in Figure 3.9. From Table A.3, the average thermal efficiency was around 52% for all the AGMD experiments shown in Condition 3. The highest one was 60%.

3.1.4 Condition 4

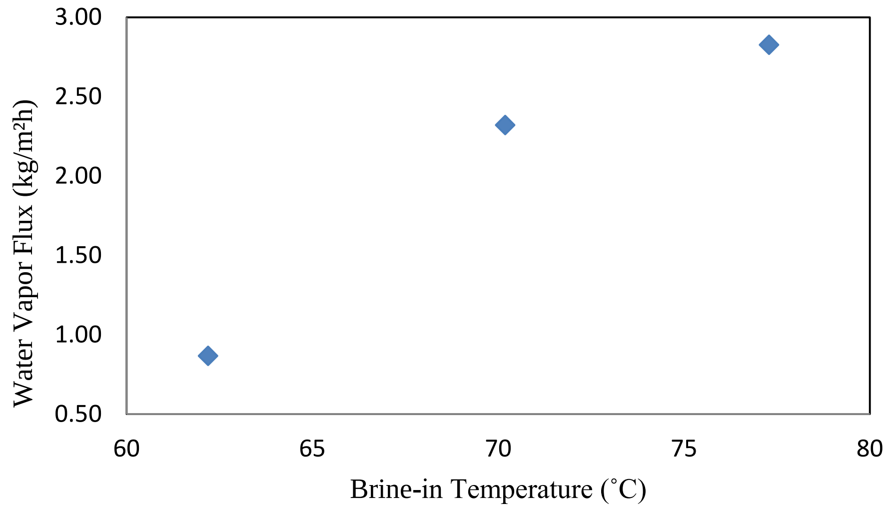

Figure 3.10 In Condition 4, the effect of brine-in temperature on water vapor flux.

For Condition 4, Modules #1 and #3 were used for AGMD and AGMD-DCMD configuration separately. Hot brine was passed through the bores of porous hollow fibers at a flow rate of 53 ml/min. Cold water was flowing through the bores of solid hollow fibers at the flow rate of 32 ml/min. Cold water temperature was maintained at about 27 ˚C for all AGMD experiments. Water vapor flux increased from 0.87 kg/m^{2}h to 2.83 kg/m^{2}h as the temperature of brine was increased from 62.2 ˚C to 77.3 ˚C shown in Figure 3.10. The thermal efficiency was as high as 63%.

3.1.5 Condition 5

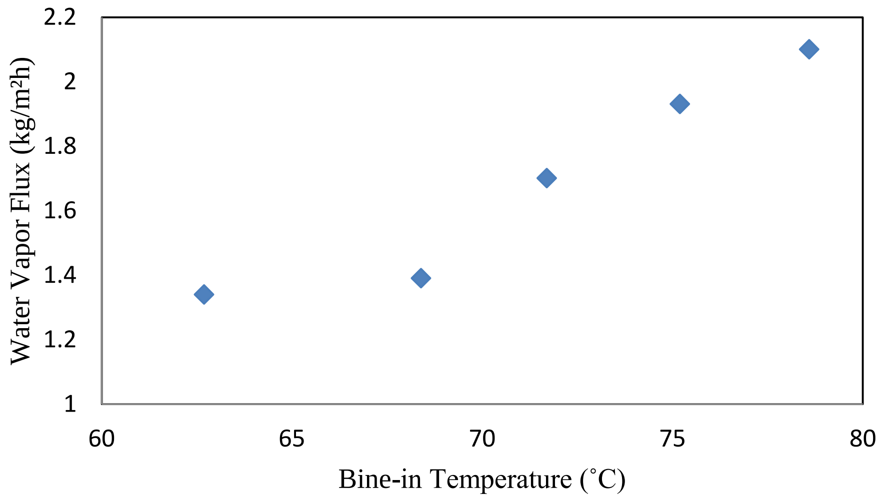

Figure 3.11 In Condition 5, the effect of brine-in temperature on water vapor flux.

For Condition 5, three modules were used. Hot brine was passed through the bores of porous hollow fibers at the flow rate of 53 ml/min. Cold water was flowing through the bores of solid hollow fibers at the rate of 32 ml/min. Cold water temperature was maintained at about 20˚C for all AGMD experiments. Water vapor flux increased from 1.34 kg/m^{2}h to 2.10 kg/m^{2}h as the temperature of brine was increased from 62.7 ˚C to 78.6 ˚C as shown in Figure 3.11. From Table A.5, the thermal efficiency was around 20% for all AGMD experiments shown under Condition 5. The highest thermal efficiency was 23%, which was much lower than one module and two modules discussed earlier.

3.1.5 Condition 6

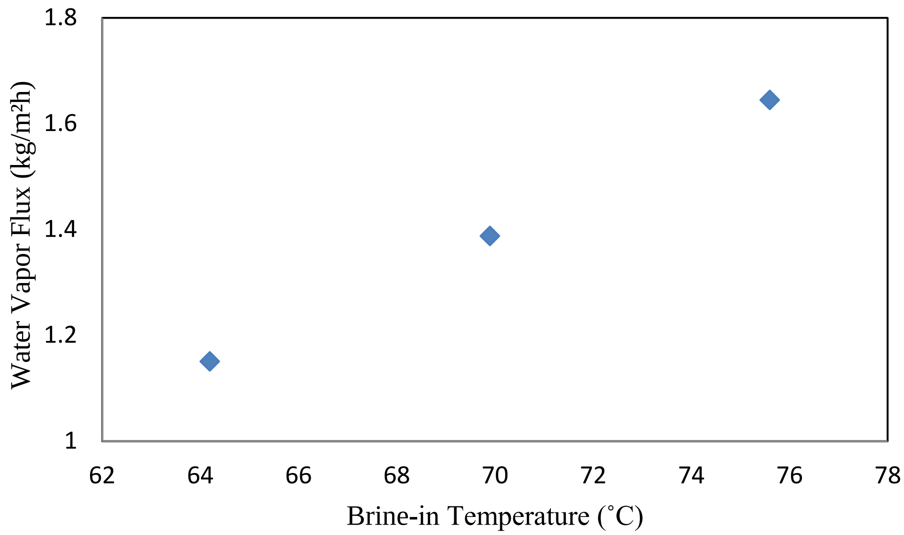

Figure 3.12 In Condition 6, the effect of brine-in temperature on water vapor flux.

For Condition 6, three modules were used. Hot brine was passed through the bores of porous hollow fibers at the flow rate of 53 ml/min. Cold water was flowing through the bores of solid hollow fibers at the rate of 34 ml/min. Cold water temperature was maintained at about 31 ˚C for all AGMD experiments. Water vapor flux increased from 1.15 kg/m^2h to 1.64 kg/m^2h as the temperature of brine increased from 64.2 ˚C to 75.6 ˚C as shown in Figure 3.12. From Table A.6, the thermal efficiency was around 34% for all AGMD experiments shown in Condition 6. The highest thermal efficiency was 36%, which was higher than Condition 5. The performances of Conditions 5 and 6 were discussed later.

3.2 Influence of Cold Water Flow Rate on Water Vapor Flux and Thermal Efficiency for Condition 5

From Figure 3.13, water vapor flux was a function of the cold water flow rate. When cold water flow rate was varied from 5 ml/min to 43 ml/min, water vapor flux was increased from 1.93 kg/m^2h to 3.04 kg/m^2h. Brine flow rate was kept at 53 ml/min, at 78 ˚C inlet temperature.

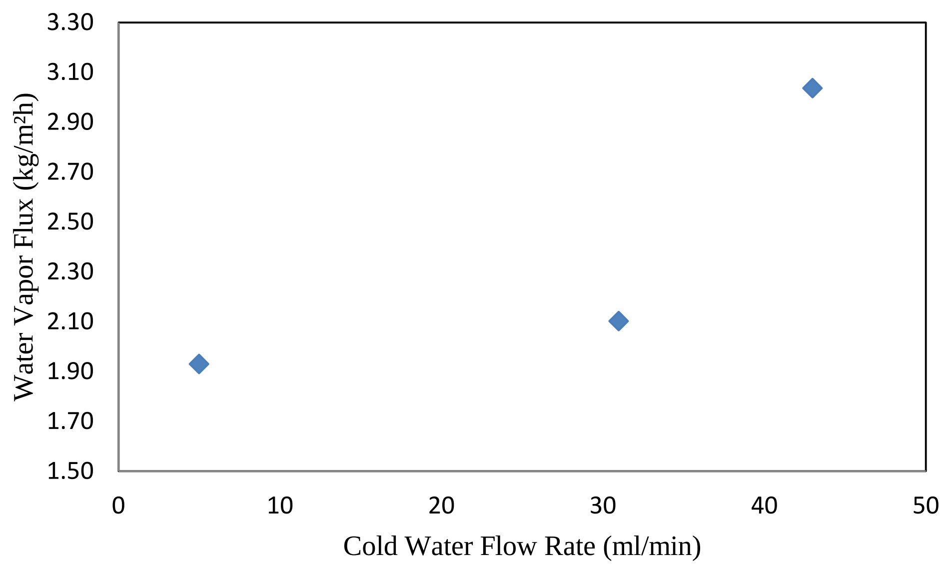

Figure 3.13 In Condition 5, the effect of cold water flow rate on water vapor flux.

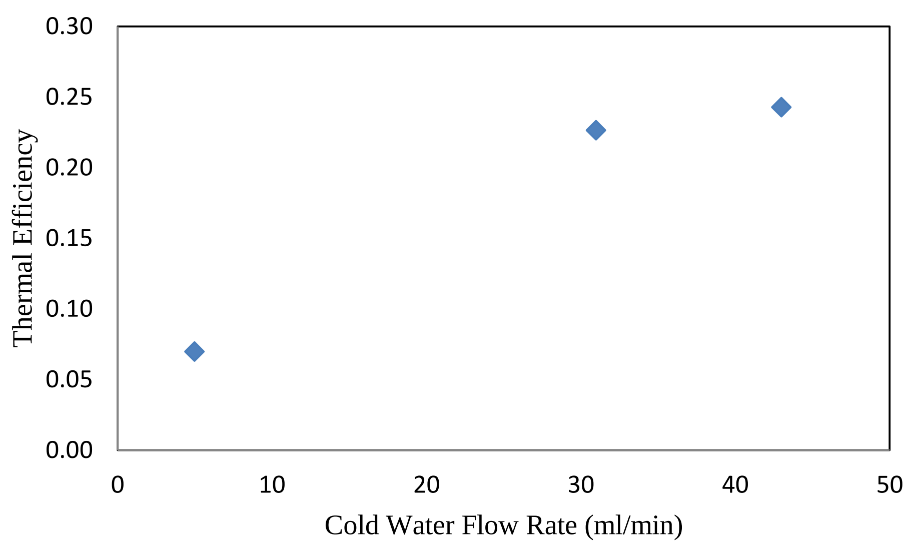

Figure 3.14 In Condition 5, effect of cold water flow rate on the thermal efficiency.

From Figure 3.14, when cold water flow rate was too low, thermal efficiency was also very low. When brine-in temperature was increased and cold water flow rate was more than 30 ml/min, thermal efficiency almost did not change and had a value of 23%.

3.3 Influence of Different Configurations on Water Vapor Flux for Conditions 2 and 3

Both Condition 2 and Condition 3 kept in series Modules #1 and #2. But they were connected in different ways. Compared with these data, the performance and efficiency of these two conditions were evaluated by using water vapor flux and thermal efficiency. From Figure 3.15, Condition 3 had higher water vapor flux when brine-in temperature changed from 53.5 ˚C to 75.7 ˚C.

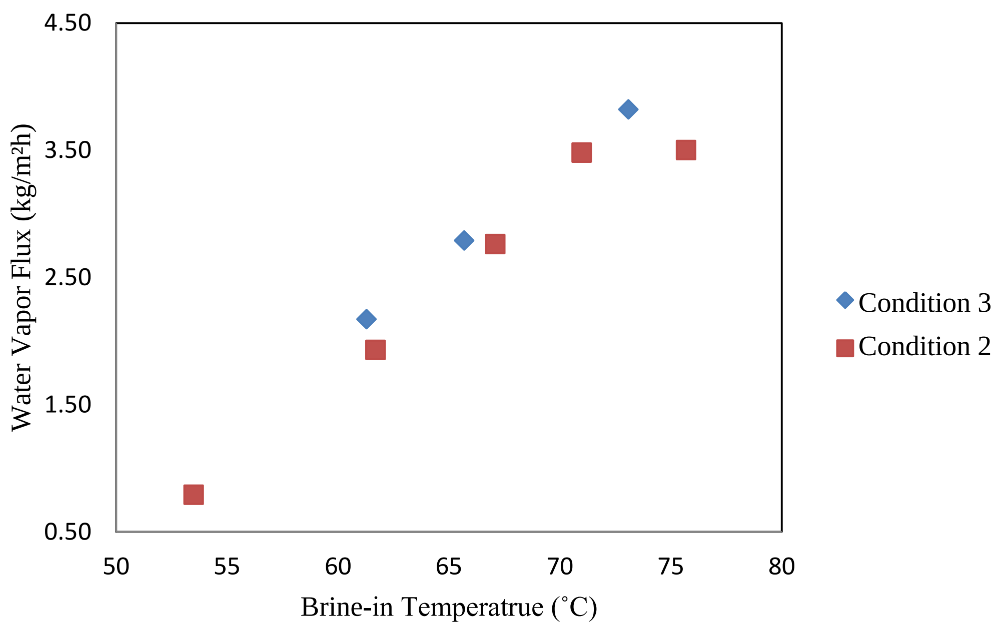

Figure 3.15 The effect of brine-in temperature on water vapor flux for Conditions 2 and 3.

3.4 Influence of Different Configurations on Water Vapor Flux for Conditions 1 and 2

For both Condition 1 and Condition 2, the water vapor flux increased with increasing brine-in temperature. But Condition 1 had higher water vapor flux than Condition 2. One module had a higher water vapor flux compared to two modules.

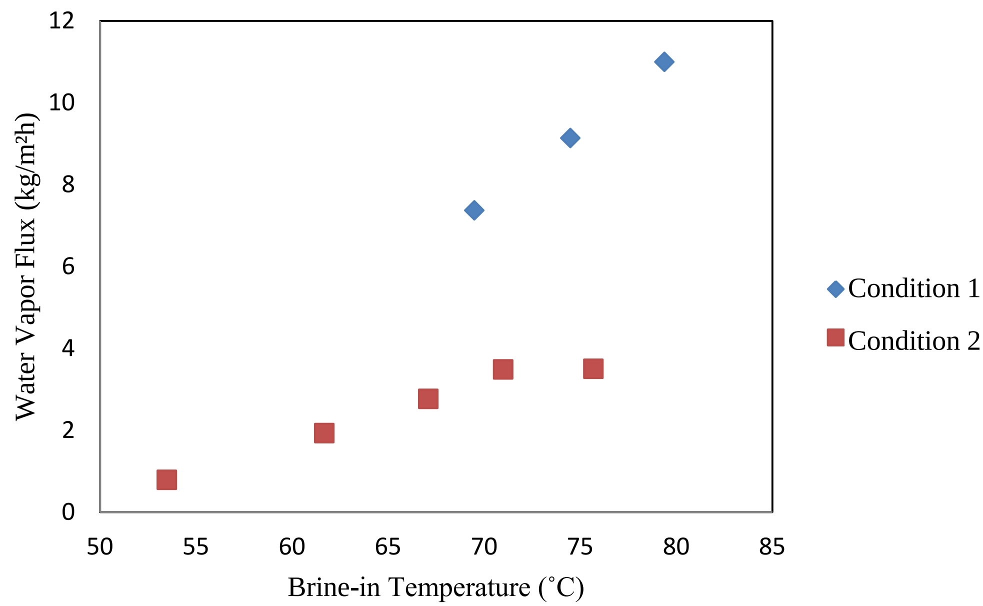

Figure 3.16 The effect of brine-in temperature on water vapor flux for Conditions 1 and 2.

3.5 Effect of Brine Flow Direction on Water Vapor Flux and Thermal Efficiency for Conditions 5 and 6

For Conditions 5 and 6, both of them were operated with three modules in series. But the brine solution entered the air gap membrane module system by different directions. For Condition 5, brine solution went through the bottom of the modules, while it flowed from top in Condition 6.

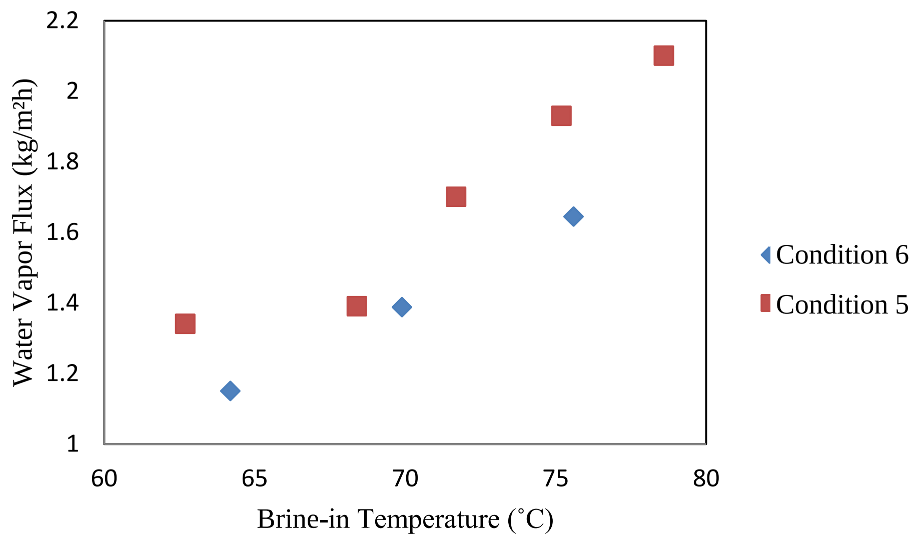

Figure 3.17 The effect of brine-in temperature on water vapor flux for Conditions 5 and 6.

For both Conditions 5 and 6, the water vapor flux increased with rising brine-in temperature from 60 ˚C to 80 ˚C. Condition 5 had higher water vapor flux than Condition 6. So when brine solution entered from the bottom of the module, it got higher water vapor flux.

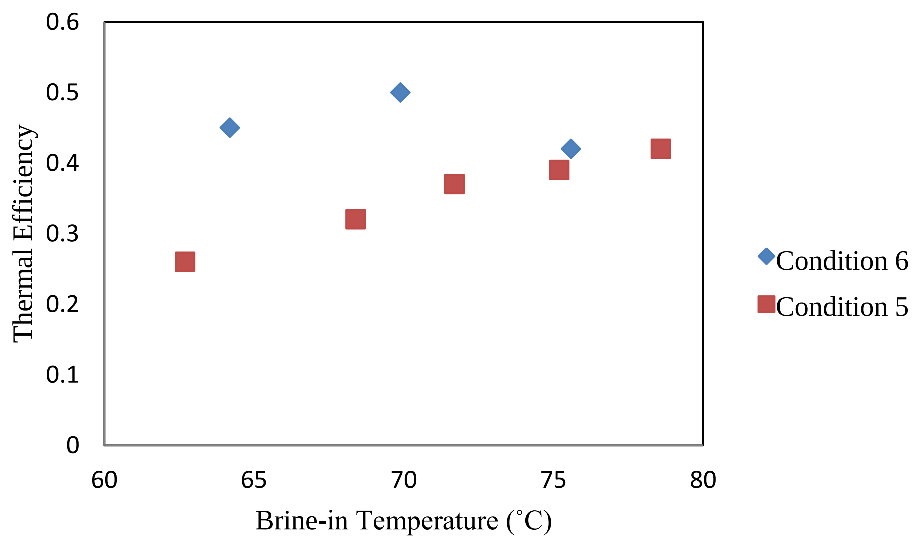

Figure 3.18 The effect of brine-in temperature on thermal efficiency in Conditions 5 and 6.

When the brine-in temperature varied from 60 ˚C to 80 ˚C, the thermal efficiency in Condition 6 was about 45%, which was higher than in the Condition 5, 35%.

CHAPTER 4

CONCLUDING REMARKS

For different configurations and connections, the water vapor flux increased with rising brine-in temperature. For Condition 5, water flux went up when the cold water flow rate increased. However when this setup was run at a very low cold water flow rate, less than 30 ml/min, the thermal efficiency became very low. It meant a huge energy loss and low operation performance. Later investigations were done for different connections for two AGMD modules. Condition 3 had higher water vapor flux compared with Condition 2. Therefore a better connection was achieved. At the same time, comparing with one AGMD module with two AGMD modules, one AGMD module had higher water vapor flux. It appeared that AGMD-DCMD configuration was used in modules having two inlets-exits, then the performances of setup were not improved. Thermal losses were partly responsible for this since series configurations had much more surface area for heat loss. Finally, through changing the stream directions of brine solution and cold water, the brine solution from the bottom of this setup had higher water vapor flux but lower thermal efficiency compared with brine entering from the top.

APPENDIX

TABLES OF ORIGINAL EXPERIMENTAL DATA

Original data of the six conditions are provided in the following tables.

Table A.1 Original Data of Condition 1

Distillate Flow Rate (kg/h)	Brine Flow Rate (ml/min)	Cold Flow Rate (ml/min)	T_{bi} (˚C)	T_{bo} (˚C)	T_{ci} (˚C)	T_{co} (˚C)	T_{cd} (˚C)	N_v (kg/m²h)	η
0.0407	76	50	69.5	54.3	19.6	31.5	32.9	7.37	0.51
0.0510	76	50	74.5	57.7	20.1	33.4	32.0	9.13	0.49
0.0567	76	50	79.4	60.1	21.9	37.2	33.0	10.99	0.51

Table A.2 Original Data of Condition 2

Distillate Flow Rate (kg/h)	Brine Flow Rate (ml/min)	Cold Flow Rate (ml/min)	T_{bi} (˚C)	T_{bo} (˚C)	T_{ci} (˚C)	T_{co} (˚C)	T_{cd} (˚C)	N_v (kg/m²h)	η
0.0062	76	50	53.5	40.3	24.7	35.8	23.7	0.79	0.52
0.0158	76	50	61.7	44.3	24.1	38.4	26.3	1.93	0.51
0.0224	76	50	67.1	45.9	24.8	40.4	28.1	2.76	0.45
0.0277	76	50	71.0	47.9	23.3	40.0	25.5	3.48	0.45
0.0278	76	50	75.7	52.6	24.9	45.0	29.1	3.50	0.54

Table A.3 Original Data of Condition 3

Distillate Flow Rate (kg/h)	Brine Flow Rate (ml/min)	Cold Flow Rate (ml/min)	T_{bi} (˚C)	T_{bo} (˚C)	T_{ci} (˚C)	T_{co} (˚C)	T_{cd} (˚C)	N_v (kg/m²h)	η
0.0179	76	50	61.3	43.1	24.2	39.7	26.1	2.25	0.52
0.0219	76	50	65.7	44.2	25.5	41.6	25.5	2.76	0.46
0.0304	76	50	73.1	50.9	25.7	47.4	26.5	3.82	0.60

Table A.4 Original Data of Condition 4

Distillate Flow Rate (kg/h)	Brine Flow Rate (ml/min)	Cold Flow Rate (ml/min)	T_{bi} (˚C)	T_{bo} (˚C)	T_{ci} (˚C)	T_{co} (˚C)	T_{cd} (˚C)	N_v (kg/m²h)	η
0.0085	53	32	62.2	32.8	27.0	38.3	23.7	0.87	0.22
0.0271	53	32	70.2	48.7	26.2	46.2	25.8	2.32	0.53
0.0340	53	32	77.3	54.5	27.3	52.6	31.8	2.83	0.63

Table A.5 Original Data of Condition 5

Distillate Flow Rate (kg/h)	Brine Flow Rate (ml/min)	Cold Flow Rate (ml/min)	T_{bi} (˚C)	T_{bo} (˚C)	T_{ci} (˚C)	T_{co} (˚C)	T_{cd} (˚C)	N_v (kg/m²h)	η
0.0189	53	31	62.7	39.1	32.3	38.0	28.1	1.34	0.14
0.0195	53	32	68.4	42.2	31.3	40.4	31.6	1.39	0.20
0.0238	53	31	71.7	43.9	34.6	46.2	32.1	1.70	0.23
0.0264	53	32	75.2	48.0	31.6	42.6	39.1	1.93	0.23
0.0359	53	31	78.6	48.6	38.3	50.2	47.7	2.10	0.23
0.0282	53	5	77.2	52.8	31.2	49.5	30.6	1.93	0.07
0.0294	53	31	78.6	48.6	38.3	50.2	47.7	2.10	0.23
0.0312	53	43	78.2	46.7	37.0	46.9	36.2	3.04	0.24

Table A.6 Original Data of Condition 6

Distillate Flow Rate (kg/h)	Brine Flow Rate (ml/min)	Cold Flow Rate (ml/min)	T_{bi} (˚C)	T_{bo} (˚C)	T_{ci} (˚C)	T_{co} (˚C)	T_1 (˚C)	T_2 (˚C)	T_3 (˚C)	N_v (kg/m²h)	η
0.0126	55	34	64.2	46.1	31.5	42.1	25.2	24.8	23.1	1.15	0.34
0.0196	55	34	69.9	48.0	30.1	43.0	22.8	25.1	22.0	1.39	0.36
0.0219	55	34	75.6	49.8	31.7	43.1	19.5	19.3	25.7	1.64	0.31

REFERENCES

[1] A. Alkhudhiri, N. Darwish, N. Hilal, Membrane distillation: A comprehensive review, Desalination 287 (2012), 2-18.

[2] R.W. Schofield, A.G. Fane, C.J.D. Fell, R. Macoun, Factors affecting flux in membrane distillation, Desalination 77 (1990), 279-294.

[3] K.W. Lawson, D.R. Lloyd, Membrane distillation, Journal of Membrane Science 124 (1997), 1-25.

[4] http://www.monzir-pal.net/Bioseparation/Lectures/L24.pdf

[5] E. Curcio, E. Drioli, Membrane Distillation and Related Operations: A Review, Separation and Purification Reviews 34 (2005), 35–86.

[6] M. E. Findley, Vaporization through porous membranes, Ind. Eng. Chem. Process Des. DeV. 6 (1967), 226.

[7] D. W. Gore, Gore-Tex membrane distillation. In Proceedings of the 10th Annual ConVention of Water Supply ImproVement Association, Honolulu, Hawaii, July (1982), 25-29.

[8] B. Li, K.K. Sirkar, Novel membrane and device for vacuum membrane distillation-based desalination process, Journal of Membrane Science 257 (2005) 60-75.

[9] L. Song, Z. Ma, X. Liao, P.B. Kosaraju, J.R. Irish, K.K. Sirkar, Pilot plant studies of novel membranes and devices for direct contact membrane distillation-based desalination, Journal of Membrane Science 323 (2008), 257-270.

[10] J. Koschikowski, M. Wieghaus, M. Rommel, Solar thermal-driven desalination plants based on membrane distillation, Desalination 156 (2003), 295-304.

[11] C.M. Guijt, G.W. Meindersma, T. Reith, A.B. de Haan, Air gap membrane distillation 1. Modelling and mass transport properties for hollow fiber membranes, Separation and Purification Technology 43 (2005), 233-244.

[12] L. Cheng, Y. Lin, J. Chen, Enhanced air gap membrane desalination by novel finned tubular membrane modules, Journal of Membrane Science 378 (2011), 398-406.

[13] D. Singh, K.K. Sirkar, Desalination by air gap membrane distillation using a two hollow-fiber-set membrane module, Journal of Membrane Science 421-422 (2012), 172-179.

[14] Z. Lei, B. Chen, Z. Ding, Membrane distillation, Special Distillation Processes, Elsevier Science, Amsterdam, Holland (2005), pp 241–319.

[15] M. Khayet, Membranes and theoretical modeling of membrane distillation: A review, Advances in Colloid and Interface Science 164 (2011), 56-88.

[16] C. Boi, S. Bandini, G.C. Sarti, Pollutants removal from wastewaters through membrane distillation, Desalination 183 (2005), 383-394.

[17] D.M. Zarkadas, K.K. Sirkar, Cooling crystallization of paracetamol in hollow fiber devices, Ind. Eng. Chem. Res. 46 (2007), 2928-2935.

[18] D. Singh, Desalination of brine and produced water by membrane distillation at lower as well as higher temperatures and pressures, PhD dissertation, New Jersey Institute of Technology (2012).